"A Theory for Strong Long-Lived Squall Lines" Revisited

MORRIS L. WEISMAN AND RICHARD ROTUNNO

National Center for Atmospheric Research, Boulder, Colorado*

(Manuscript received 29 April 2002, in final form 7 August 2003)

ABSTRACT

Based on the analysis of idealized two- and three-dimensional cloud model simulations, Rotunno et al. (hereafter RKW) and Weisman et al. (hereafter WKR) put forth a theory that squall-line strength and longevity was most sensitive to the strength of the component of low-level (0–3 km AGL) ambient vertical wind shear perpendicular to squall-line orientation. An ''optimal'' state was proposed by RKW, based on the relative strength of the circulation associated with the storm-generated cold pool and the circulation associated with the ambient shear, whereby the deepest leading edge lifting and most effective convective retriggering occurred when these circulations were in near balance. Since this work, subsequent studies have brought into question the basic validity of the proposed optimal state, based on concerns as to the appropriate distribution of shear relative to the cold pool for optimal lifting, as well as the relevance of such concepts to fully complex squall lines, especially considering the potential role of deeper-layer shears in promoting system strength and longevity. In the following, the basic interpretations of the RKW theory are reconfirmed and clarified through both the analysis of a simplified two-dimensional vorticity–streamfunction model that allows for a more direct interpretation of the role of the shear in controlling the circulation around the cold pool, and through an analysis of an extensive set of 3D squall-line simulations, run at higher resolution and covering a larger range of environmental shear conditions than presented by WKR.

1. Introduction

The association of squall lines with environmental vertical wind shear has been recognized since routine upper-air soundings first became available (e.g., Byers and Braham 1949; Newton 1950; Bluestein and Jain 1985). Indeed, numerical modeling studies (e.g., Hane 1973; Thorpe et al. 1982; Rotunno et al. 1988, hereafter RKW; Weisman et al. 1988, hereafter WKR; Fovell and Ogura 1989; Robe and Emanuel 2001) show that simulated squall lines depend critically on the ambient vertical wind shear. Using a two-dimensional numerical model, Thorpe et al. (1982) noted more specifically that simulated squall lines were strongest for environments in which the vertical shear was confined to low levels. RKW and WKR noted a similar dependence of squall-line strength and longevity on the wind shear, using both two- and three-dimensional simulations, and observed that the simulated squall line was maintained through the regeneration of new cells along a line of cold outflow produced during the decay of old cells. RKW found that the ability of the cold surface outflow of an old cell to lift environmental boundary layer air to its level of free convection (and so produce a new cell) is enhanced with low-level shear, and concluded that the cold-pool–shear interaction is a central element in understanding the maintenance of strong squall lines in the absence of significant external forcing features (e.g., cold fronts, etc.). Critics of the RKW theory of squall lines have charged that the focus on the cold-pool–shear interaction is an oversimplification as it neglects the larger-scale squall-line circulations (e.g., Lafore and Moncrieff 1989; Garner and Thorpe 1992). Others (e.g., Coniglio and Stensrud 2001; Evans and Doswell 2001) contend that, upon closer inspection, observations and models do not support such a strong connection between low-level shear and squall-line characteristics. Still others have put forth alternative theories to explain the deep lifting induced by the cold-pool–shear interaction (e.g., Xu 1992; Xu and Moncrieff 1994; Xu et al. 1996, 1997; Xue 2000). The present paper addresses these issues.

The RKW theory of squall lines is fundamentally concerned with how typical thunderstorms, which undergo a 30–50-min life cycle (e.g., Byers and Braham 1949), can be regenerated along a line. RKW proposed a simple way of thinking about how low-level shear enhances the regeneration process: For a cold pool spreading in an environment without shear (Fig. 1a), the circulation at the leading edge is as described for a classic density current (e.g., Simpson 1997), with the

* The National Center for Atmospheric Research is sponsored by the National Science Foundation.

Corresponding author address: Morris L. Weisman, NCAR, P.O. Box 3000, Boulder, CO 80307-3000.
E-mail: weisman@ncar.ucar.edu

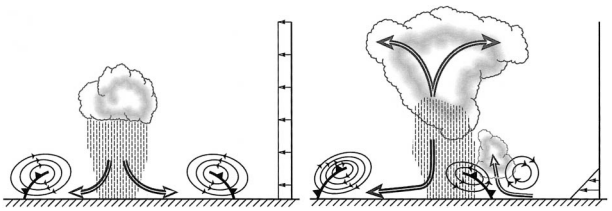

FIG. 1. (left) Cold pool spreads away from a decaying convective cell in an environment with no vertical wind shear. (right) Low-level vertical wind shear balances cold-pool circulation on the downshear side, enhancing the ability to regenerate convective cells through deeper lifting.

environmental air being forced up and over a deeper head region, and then subsiding over the main body of cold air. When ambient shear is present (Fig. 1b), the circulation associated with the shear will, on the downshear side, counteract some of the circulation associated with the cold pool, producing deeper lifting there. The deepest lifting and largest potential for cell retriggering occurs when the cold pool and shear circulations are in balance. Naturally, the shear layer occupying the same vertical levels as the cold pool was proposed to be the most important for this effect. This basic impact of shear on a density current has been reproduced in many other recent studies (e.g., Xu et al. 1996, 1997; Xue 2000), although differing interpretations of the effect have been offered, as is discussed below.

The RKW cold-pool–shear interaction theory addresses the threshold question of how the shear affects the transformation of ordinary finite-lifetime thunderstorms into a long-lasting system of cells continually regenerating along a line. Our view is that only after this threshold question has been answered, does it make sense to consider questions concerning the collective effects of many generations of cells. For example, mature squall lines often have a rear-inflow jet (e.g., Smull and Houze 1987) which, according to numerical simulations, can originate through the collective heating/cooling pattern of the convective cells (Lafore and Moncrieff 1989; Weisman 1992). Consider the evolution of a squall-line circulation as presented schematically in Fig. 2, where C is a velocity representing the strength of the cold pool and Δu represents the magnitude of the low-level ambient vertical wind shear. Before a significant cold pool develops ($C \ll \Delta u$), the convective cells within the squall line tilt predominantly in a downshear direction in response to the ambient shear (Fig. 2a); after a cold pool has developed, its circulation may counter that associated with the low-level shear to produce deeper lifting at low levels and an overall more upright convective structure ($C \sim \Delta u$, Fig. 2b); finally, if the cold pool evolves to a state where $C > \Delta u$, then the circulation associated with the cold pool dominates that of the shear, thereby sweeping the convective cells and associated zone of heating/cooling rearward (toward the left in the figure), where it can induce the generation of a rear-inflow jet (Fig. 2c). The RKW ''optimal'' state

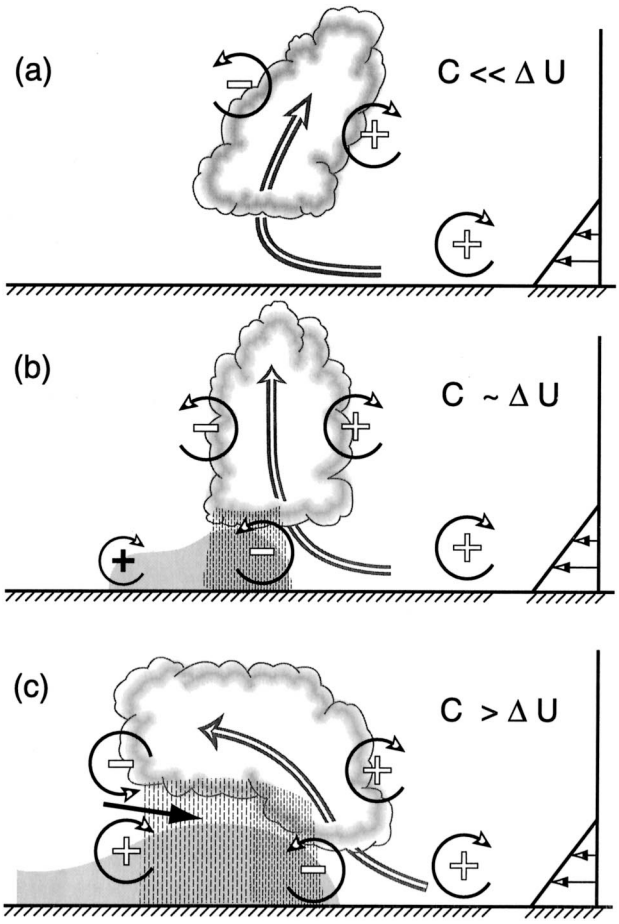

FIG. 2. Three stages in the evolution of a convective system. (a) An initial updraft leans downshear in response to the ambient vertical wind shear, which is shown on the right. (b) The circulation generated by the storm-induced cold pool balances the ambient shear, and the system becomes upright. (c) The cold-pool circulation overwhelms the ambient shear and the system tilts upshear, producing a rear-inflow jet. The updraft current is denoted by the thick, double-lined flow vector, and the rear-inflow current in (c) is denoted by the thick solid vector. The shading denotes the surface cold pool. The thin, circular arrows depict the most significant sources of horizontal vorticity, which are either associated with the ambient shear or which are generated within the convective system, as described in the text. Regions of lighter or heavier rainfall are indicated by the more sparsely or densely packed vertical lines, respectively. The scalloped line denotes the outline of the cloud. Here, C represents the strength of the cold pool while Δu represents the strength of the ambient low-level vertical wind shear, as described in the text (adapted from Weisman 1992).

is envisioned when $C/\Delta u$ is close to 1, whereby the system maintains an upright configuration and the deepest lifting is produced at the leading edge of the cold pool. However, for all except the most strongly sheared environments, squall lines tend to evolve through all three depicted phases during their lifetimes, as cold pools usually strengthen over time and eventually become strong enough to overwhelm the ambient shear.

The induced rear-inflow circulation during the mature phase of a squall line might fundamentally alter the

original conditions allowing continual cell regeneration. However, based on the analysis of an extensive set of quasi-three-dimensional squall-line simulations, WKR and Weisman (1992) showed that the dependence of squall-line structure, strength, and longevity on environmental vertical wind shear could still be largely explained based on the simple cold-pool–shear interaction ideas. WKR considered both the ability of a system to maintain upright convective cells along the leading edge of the gust front for long periods, and also the total condensation produced within the convective system. By both measures, the optimal squall lines occurred for environments with moderate-to-strong vertical wind shear confined to the lowest 2.5 km AGL and oriented perpendicular to the squall line. Deeper layers of strong shear were able to support the development of strong, isolated cells scattered along the line (some of which were supercellular), but were not as effective as the shallower shear layers in producing a continuous line of updrafts. Weisman (1993) and Weisman and Davis (1998) further showed that strong low-level shears were especially conductive to the development of three-dimensional bow-shaped segments embedded within such lines, with attendant ''bookend'' or ''line-end'' vortices at midlevels (e.g., 2–6 km AGL) with attendant locally intense rear-inflow jets that could further enhance system strength.

Although there is general agreement among the modeling studies that low-level shear is important, there is less agreement on why it is important, and moreover, its importance relative to other factors. In diagnosing simulations of tropical squall lines, Lafore and Moncrieff (1989) emphasized that, in contrast with RKW, it is the differential speed of the cold pool versus the convective cells that is the more critical factor in system morphology (reinforcing the interpretation of Thorpe et al. 1982; see also Moncrieff and Liu 1999), and therefore suggested that ''the wind shear in the entire troposphere should be considered in the interaction of the cold pool and the convective cells.'' They also noted that system-scale circulation features, such as the above discussed rear-inflow jets, contribute significantly to mature squall-line structure, stating further that ''it is an oversimplification to say that the interaction of the shear and the cold pool adequately explains the longevity of mesoscale convective systems because the organization of the vorticity field is predominantly on the scale of the entire system and not confined to a localized convection scale.'' This issue of ''local'' versus ''global'' effects is summarized in Lafore and Moncrieff (1990), where they emphasize that many factors, such as the upstream effects of the squall line, which can modify the low-level shear, the wind profile in mid- to upper levels, the differential movement of convective cells, and synoptic-scale effects all can have a significant impact on system morphology. Thus, they conclude: ''Local vorticity balance is an interesting concept, but its importance to squall line convective systems, relative to the more complex processes listed above, remains unresolved.''

Using a composite environment for observed severe, long-lived convective wind storms (referred to as derechos), Coniglio and Stensrud (2001) employed a mesoscale forecast model with mesoscale variability in the environmental conditions, and successfully simulated many of the essential characteristics of such systems. They noted, however, that the system maintained convective cells along the gust front for much longer periods than the squall lines presented in WKR and Weisman (1993) for similar low-level vertical wind shear, and noted further that the deeper-layer shear in this case may have been critical for the strength and sustenance of the simulated system. Evans and Doswell (2001) completed a climatological study of environments associated with widespread convectively produced windstorms, and also found that such events could occur for weaker magnitudes of low-level vertical wind shear than suggested in previous simulations of WKR and Weisman (1993).

The goal of the present paper is to revisit the RKW theory that squall-line strength and longevity are especially enhanced in the presence of moderate-to-strong low-level vertical wind shear and that the process by which this happens is through shear-enhanced lifting by cool pools. To accomplish this goal, in the following section we revisit the primary building block of the RKW theory, that cold-pool lifting is especially enhanced by low-level shear. This will be addressed by presenting new results from a two-dimensional vorticity–streamfunction model of a density current spreading in a sheared environment; numerical experiments are done to demonstrate the effects on cold-pool lifting of shallow versus deep shear, and of surface-based versus elevated shear. The new model also allows for a more direct interpretation of this enhancement in terms of a relative balance between the circulation associated with the cold pool and that associated with the shear, as originally presented by RKW. In section 3, we will reconsider the degree to which the cold-pool–shear interaction explains the behavior of full, three-dimensional squall-line simulations, through the analysis of an extensive set of new idealized simulations, with enhanced resolution on larger domains, which extend the results of WKR to include both deeper and elevated shear layers. Section 4 contains further discussion and a summary.

2. Cold pools spreading in shear flow

At the time of the writing of RKW, there was only one paper in the literature explicitly recognizing that ambient vertical wind shear adds a fundamentally new element to the dynamics of density currents (Jirka and Arita 1987). Reasoning through the vorticity equation, RKW argued that deeper lifting should be expected where the circulation of the cold pool is opposed by that associated with the shear (cf. Fig. 1b). Shortly after

RKW, a series of papers beginning with Xu (1992) looked at steady-flow solutions of gravity currents in ambient shear contained in a channel of finite depth. Xu (1992) used overall mass and momentum balance as a way of deducing the height of the gravity current at a large distance from its leading edge $h_{-\infty}$. Xu and Moncrieff (1994), following the same methodology, consider the effects of circulations within the cold pool on $h_{-\infty}$. In both of these studies the height of the cold pool at the leading edge is considered to be outside the realm of the theoretical calculations. Numerical simulations by Xu et al. (1996) of gravity currents in an environment of constant ambient shear showed the expected result of deeper currents with shear than without. However as stated in of Xu et al. (1996, p. 771), ''As in the [above cited] theoretical models, the rigid upper boundary used in our numerical study plays an important role in keeping the simulated density currents quasi steady . . .'' Xue et al. (1997) extend the simulations of Xu et al. (1996) to the case of gravity currents with the ambient shear restricted to low levels. Xue et al. (1997) acknowledge that ''Similar to the numerical experiments of RKW, these experiments show that the slope of the frontal interface, the depth of the density current . . . are controlled by the shear of the low-level inflow.'' However, the effects are analyzed in terms of the steady-flow models, which as stated in Xu et al. (1996), are heavily influenced by the upper rigid lid. In the following, we present calculations of cold pools spreading in shear based on the vorticity–streamfunction version of the equations of motion. These calculations show that the RKW ideas, based on vorticity reasoning, are both qualitatively and quantitatively accurate, and are not limited to steady-state flows of the type considered in the above-cited work.

The formulation of the problem is motivated by the phenomenology depicted in Fig. 1a: rain from a decaying thunderstorm cell quickly chills and loads the air below it. Hence the fluid mechanical problem is to determine the way the cold air spreads at the ground and how this spreading is affected by ambient shear. To study this problem in a manner consistent with the ideas developed in RKW, a simple two-dimensional vorticity–streamfunction model has been devised.

The governing equations for two-dimensional flow in the $\tilde{x}$–$\tilde{z}$ plane are

$$\frac{d\tilde{\eta}}{d\tilde{t}} = -\partial_{\tilde{x}}\tilde{b} + \tilde{\nu}\tilde{\nabla}^2\tilde{\eta}, \tag{1}$$

$$\frac{d\tilde{b}}{d\tilde{t}} = \tilde{\nu}\tilde{\nabla}^2\tilde{b}, \quad \text{and} \tag{2}$$

$$\tilde{\nabla}^2\tilde{\psi} = \tilde{\eta}, \tag{3}$$

where $\tilde{b}$ is the buoyancy, $\tilde{\eta}$ the $\tilde{y}$ component of vorticity, $\tilde{\psi}$ the streamfunction, and $\tilde{\nu}$ the kinematic viscosity. The material derivative $d/dt = \partial_{\tilde{t}} + \tilde{u}\partial_{\tilde{x}} + \tilde{w}\partial_{\tilde{z}}$, where the velocity $(\tilde{u}, \tilde{w}) = (\partial_{\tilde{z}}\tilde{\psi}, -\partial_{\tilde{x}}\tilde{\psi})$. Here and throughout this section all symbols with a tilde denote dimensional variables.

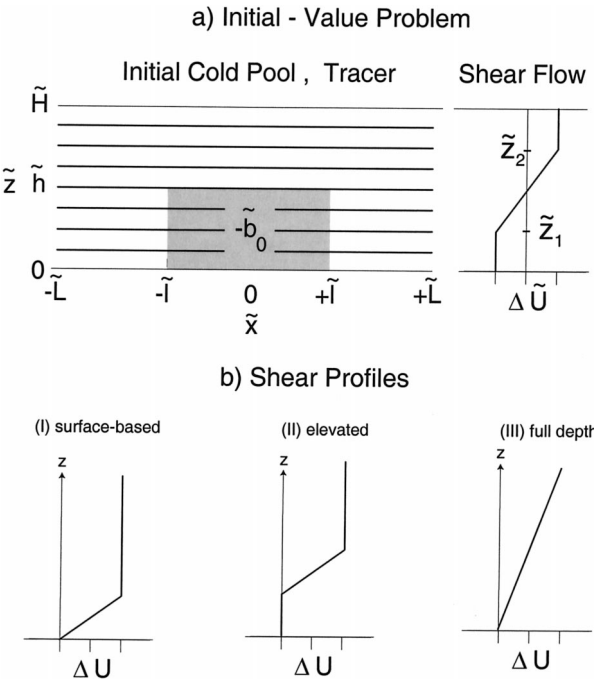

FIG. 3. (a) Initial condition for two-dimensional cold-pool-in-shear simulations. Shaded region represents uniform block of cold air; horizontal lines indicate initial tracer field; definition of the initial shear layer is indicated. (b) The three shear profiles used in the simulations.

The basic flow to be analyzed is shown in Fig. 3a: there is at $\tilde{t} = 0$ a block of cold air described by the function

$$\tilde{b} = \begin{cases} -\tilde{b}_0, & |\tilde{x}| < \tilde{l},\ \tilde{z} < \tilde{h} \\ 0, & \text{otherwise} \end{cases} \tag{4}$$

contained within a channel of depth $\tilde{H}$ and length $\tilde{L}$. The initial vorticity (associated with the ambient shear flow shown in Fig. 3a; profiles used here are illustrated in Fig. 3b) is

$$\tilde{\eta} = \begin{cases} \tilde{\eta}_0, & \tilde{z}_1 \le \tilde{z} \le \tilde{z}_2 \\ 0, & \text{otherwise} \end{cases} \tag{5}$$

where $\tilde{\eta}_0 = \Delta\tilde{U}/(\tilde{z}_2 - \tilde{z}_1)$; $\tilde{b}_0$ and $\tilde{\eta}_0$ are constants. The boundary conditions are $\tilde{w} = \partial_{\tilde{z}}\tilde{b} = \partial_{\tilde{z}}\tilde{\eta} = 0$ at $\tilde{z} = 0$, $\tilde{H}$ and, for simplicity, periodicity at large distance $\tilde{x} = \pm\tilde{L}$.

Dimensional analysis says that the solution can depend on seven nondimensional parameters, which we identify as follows:

$$\frac{\Delta\tilde{U}}{\sqrt{\tilde{b}_0\tilde{h}}}, \quad \frac{\Delta\tilde{z}}{\tilde{h}}, \quad \frac{\tilde{z}_m}{\tilde{h}}, \quad \frac{\tilde{\nu}}{\tilde{h}\sqrt{\tilde{b}_0\tilde{h}}}, \quad \frac{\tilde{l}}{\tilde{h}}, \quad \frac{\tilde{H}}{\tilde{h}}, \quad \frac{\tilde{L}}{\tilde{h}}, \tag{6}$$

where $\Delta\tilde{z} = \tilde{z}_2 - \tilde{z}_1$ and $\tilde{z}_m = (\tilde{z}_2 + \tilde{z}_1)/2$.

Equations (1)–(5) are next nondimensionalized using $\tilde{h}$ as the length scale, $\tilde{b}_0$ as the buoyancy scale, $\sqrt{\tilde{b}_0\tilde{h}}$

as the velocity scale, and $\tilde{h}/\sqrt{\tilde{b}_0\tilde{h}}$ as the time scale. The result is

$$\frac{d\eta}{dt} = -\partial_x b + \nu\nabla^2\eta, \tag{1'}$$

$$\frac{db}{dt} = \nu\nabla^2 b, \tag{2'}$$

$$\nabla^2\psi = \eta, \tag{3'}$$

$$b = \begin{cases} -1, & |x| < l,\ z < 1 \\ 0, & \text{otherwise, and} \end{cases} \tag{4'}$$

$$\eta = \begin{cases} \eta_0, & z_1 \le z \le z_2 \\ 0, & \text{otherwise,} \end{cases} \tag{5'}$$

where $\eta_0 = \Delta U/\Delta z$, and $\nu = \tilde{\nu}/(\tilde{h}\sqrt{\tilde{b}_0\tilde{h}})$. The boundary conditions are $w = \partial_z b = \partial_z \eta = 0$ at $z = 0$, H and periodicity at $x = \pm L$. Symbols without a tilde are the nondimensional variables corresponding to the dimensional ones defined above. The model domain $(x, z) \in (-L, +L) \times (0, H)$ is resolved with $nx \times nz = 960 \times 80$ uniform grid increments. Equations (1′)–(3′) are discretized on a nonstaggered grid using second-order-accurate finite differencing in space and advanced in time through the leapfrog technique; the Poisson equation (3) is solved using the National Center for Atmospheric Research (NCAR) library routine POIS.

The choices for the parameters in (6) are guided by the following considerations. The cloud model simulations show that the cell-triggering lifting at the leading edge of the surface outflow occurs perforce as soon as the surface outflow is generated. Thus we focus here on the evolution of the cold pool over short times choosing the domain large enough so that it exerts no significant influence on the flow; here we take $L = 12$, $H = 2$ and will present evidence that these are large enough. In the absence of initial shear the problem described in Fig. 3 is the so-called dam-break problem (e.g., Stoker 1957). Solutions of the shallow-water equations indicate that, after the dam breaks, the steady outflow from the reservoir is accompanied by a depression wave traveling into the reservoir at speed $\sqrt{\tilde{b}_0\tilde{h}}$. With two dams breaking (as in Fig. 3a), there will be a constant supply of fluid to the outflow until the depression waves from both dams meet, reflect, and travel back to the dam sites, that is, until $t = 2\tilde{l}/\tilde{h}$. We take $\tilde{l} = 2\tilde{h}$ and, guided by the dam-break problem, integrate Eqs. (1′)–(3′) over $t \in (0, 4)$ with a uniform time step of $dt = 0.01$. It is also known from past studies that a characteristic feature of the outflow is turbulent motion at its top. Thus, we take $\nu = 0.002$, which is large enough to control the small-scale instability that occurs in the inviscid problem, but small enough to preserve the large-scale character of the solutions. With the latter four parameters of (6) specified, we investigate the dependence of the solution on the first three parameters in (6).

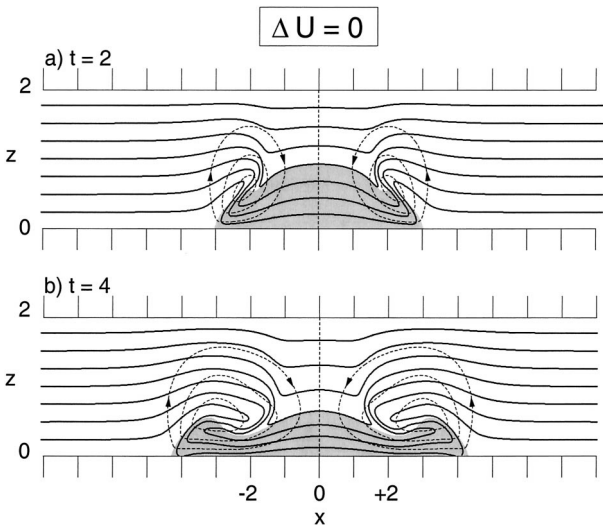

FIG. 4. Collapse of a cold pool with zero initial shear ($\Delta U = 0$) at (a) $t = 2$ and (b) $t = 4$. Here and subsequently, the shaded region denotes the area where the buoyancy $b < -0.5$; contours of streamfunction ψ (interval = 0.1) are indicated by the dashed lines; the heavy solid lines indicate the contours of the tracer field s (interval = 0.25).

a. Density current-shear simulations

Consider first in Fig. 4 the collapse of the initial cold pool in the absence of ambient shear. The shaded region represents values of $b < -0.5$ and the streamfunction ψ is indicated in dashed lines with contour interval = 0.1. To keep track of the vertical displacement of low-level air parcels, we define a tracer s such that it obeys the same equation and boundary condition as b (2′), but with initial condition $s(x, z, 0) = z$. It is clear from (1′) that vorticity of opposite signs is generated at the lateral edges of the initial cold pool; the generated vorticity implies a flow by (3′) that sinks and spreads the cold air while raising the surrounding low-level air parcels. [In all simulations the cold pool is well contained within the domain $x \in (-12, +12)$ at $t = 4$.] By comparing the value of s over the cold air with its undisturbed value and restricting attention to parcels for which $s < 0.5$, we have a precise measure of the maximum vertical displacement of low-level air parcels. Figure 5 shows $\delta_m \equiv \{\max(z - s);\ s < 0.5\} \approx 0.5$ for $\Delta\tilde{U}/\Delta\tilde{z} = 0$ at the simulation end time $t = 4$ (case A).

Three distributions of ambient velocity are studied here (see Fig. 3b):

1) Surface-based, limited-depth shear layer

   $z_m = 0.25, \quad \Delta z = 0.5, \quad \Delta U = 0.25$ to 1.5.

2) Limited-depth shear layer centered at the initial cold-pool top

   $z_m = 1.0, \quad \Delta z = 0.5, \quad \Delta U = 0.25$ to 1.5.

3) Shear layer over the entire depth

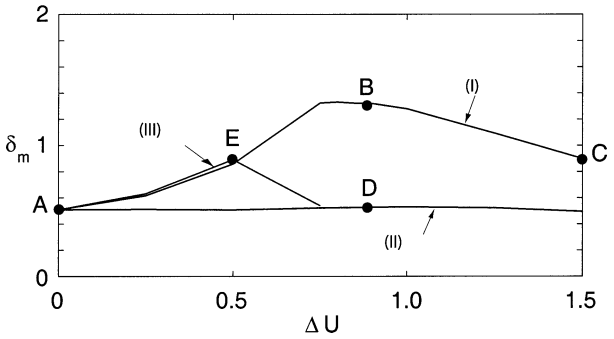

FIG. 5. The maximum displacement (δ_m) of low-level ($s < 0.5$) air parcels at $t = 4$ for all experiments. Letters indicate solutions displayed in Figs. 4 and 6–9. The three curves correspond to the shear profiles shown in Fig. 3b.

$$z_m = 1.0, \qquad \Delta z = 2.0, \qquad \Delta U = 1.0, 2.0, 3.0.$$

The choice of ΔU in shear profile (iii) is made so that $\Delta U/\Delta z$ is the same as it is in cases (i) and (ii) for $\Delta U = 0.25$, 0.5, and 0.75.

The maximum low-level displacement δ_m at $t = 4$ for all of these cases is shown in Fig. 5. For shear profile (i), there is clearly a shear that produces the maximum lift. Figure 6 shows the case with $\Delta U = 0.85$ (case B); the effect of the shear is evident at $t = 2$ as it tends to tilt the initial cold block downshear. However, by $t = 4$ this tendency is opposed by the cold-pool circulation on the downshear edge and deep lifting occurs. Figure 7 shows the solution for shear profile (i) with $\Delta U = 1.50$ (case C); in this case the downshear tilting of the cold pool is too strong for the cold-pool-generated circulation to overcome and the lifting is not as deep.

There has been some discussion in the literature on whether the low-level shear is the most important feature of the shear distribution in determining the ability of the cold pool to lift air parcels (Xue 2000). Figure 5 shows that with the shear layer displaced to the top of the original cold pool (ii), the effect on the low-level lifting is negligible. We have done experiments with the shear-layer place at intermediate levels ($0.0 < z_m < 0.5$, $\Delta z = 0.5$) and find a monotonic transition from no effect on lifting with shear profile (ii) to the strong effect associated with shear profile (i). In a description of an elevated shear-layer numerical experiment, RKW (p. 477) said that it is only the shear layer that ''makes contact with'' the cold pool that matters for enhanced lifting. The latter phrase is technically incorrect since, as just stated, the vorticity of even a marginally elevated shear layer still has an associated circulation which acts at a distance [cf. Eq. (3)] to produce enhanced lifting. The phrase should have been ''in close proximity to'' which would have made it consistent with the action-at-distance argument made in the same paragraph (RKW, p. 477; see the italicized phrase). Figure 8 shows the simulation from shear profile (ii) with $\Delta U = 0.85$, indicating that there is no significant extra lifting of low-level air beyond that obtained with zero ambient shear (Fig. 4) with the shear layer elevated completely above the cold pool.

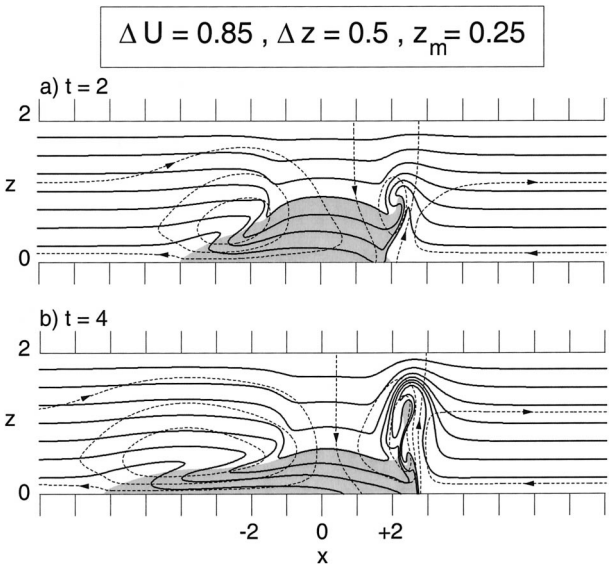

FIG. 6. As in Fig. 4 except $\Delta U = 0.85$, $\Delta z = 0.5$, and $z_m = 0.25$.

Finally there have been a number of analytical and numerical studies (e.g., Xu et al. 1996) which have examined the case of uniform shear over the domain depth. Figure 5 shows that the lifting associated with a deep shear profile (iii) is similar to that of a surface-based limited-shear profile (ii) for $\Delta U/\Delta z < 1$; however, beyond that value the lifting is reduced, indicating that deep-layer shear is detrimental. Figure 9 shows the simulation from (iii) with $\Delta U = 2.0$ (case E). It was also noted by Xu et al. (1996, p. 771) that the upper lid plays an important role in their solutions. The simulations

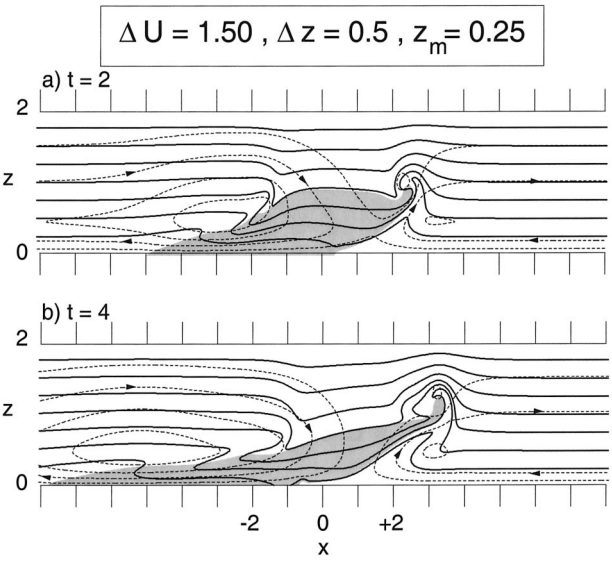

FIG. 7. As in Fig. 4 except $\Delta U = 1.5$, $\Delta z = 0.5$, and $z_m = 0.25$.

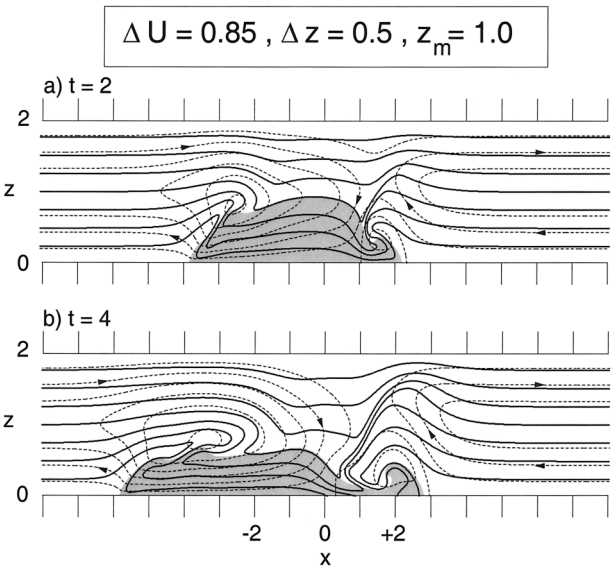

FIG. 8. As in Fig. 4 except $\Delta U = 0.85$, $\Delta z = 0.5$, and $z_m = 1.0$.

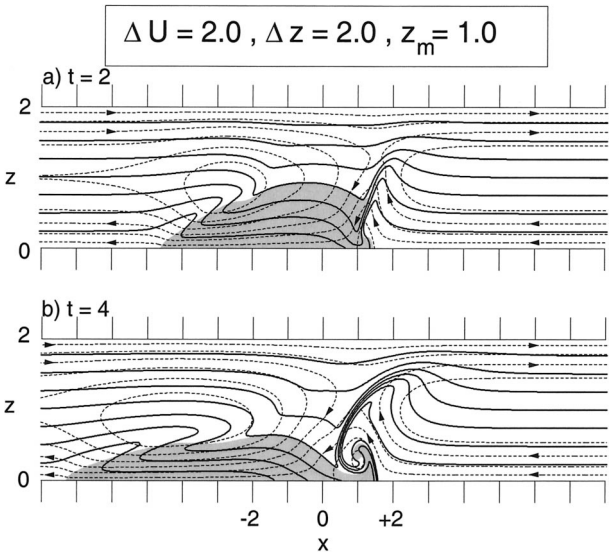

FIG. 9. As in Fig. 4 except $\Delta U = 2.0$, $\Delta z = 0.5$, and $z_m = 0.25$.

discussed above were repeated with the vertical domain size doubled ($H = 4$) and there was no significant effect on the displacements shown in Fig. 5.

b. Vorticity dynamics

The displacement of an air parcel is defined by the equation

$$\frac{d\delta}{dt} = w. \tag{7}$$

Equation (7) says that an air parcel will experience more vertical displacement when it resides in a region of $w > 0$ for a longer time. A simple explanation based on vorticity dynamics [(1′)–(3′)] for the effect of shear on the lifting ability of a spreading cold pool was given in RKW (sections 4a,b). With zero ambient shear, Fig. 4 shows that lifted air is rapidly swept rearward of the cold-pool leading edge by the circulation associated with baroclinically generated vorticity; air parcels reside in the updraft region for a relatively short time. Figure 6 suggests that the circulation associated with the ambient shear counters (on the downshear side) that associated with the baroclinically generated vorticity and, consequently, air parcels reside in the updraft region for a relatively long time. With larger amounts of shear (Fig. 7), fluid parcels spend less time in the updraft, and the vertical displacement is less again. A quantitative analysis confirming the above ideas is shown in Fig. 10; Fig. 10a presents the full streamfunction (ψ) for the case of maximum δ_m shown in Fig. 6. In Fig. 10b, the streamfunction represents the flow associated only with $\eta < 0$ (the vorticity produced by the downshear cold pool) while Fig. 10c shows that associated only with $\eta > 0$ (the mean shear vorticity plus the vorticity produced by the upshear cold pool). The nearly balancing tendencies of both on the downshear side of the cold pool is apparent.

c. Summary

Enhanced lifting at the downshear edge of the cold pool was identified by RKW as a major contribution to the strength and longevity of squall lines. RKW's original analysis was made in terms of the two-dimensional equations of motion in the streamfunction–vorticity form. Here we have solved these equations numerically to reconfirm the importance of the low-level shear and to show that the qualitative arguments of RKW are quantitatively accurate. The argument is that the deepest lifting occurs when the circulation associated with the cold pool is nearly balanced with that of the low-level shear. By a simple control volume analysis RKW deduced that this balance occurs when

$$\Delta\tilde{U} = \sqrt{2\tilde{b}_0\tilde{h}_c} \equiv C, \tag{8}$$

where $\tilde{h}_c$ is the height of the cold pool. Examination of Fig. 6 shows that $\tilde{h}_c \approx \tilde{h}/2$, and so (8) gives $\sqrt{\tilde{b}_0\tilde{h}}/\Delta\tilde{U} = 1$, which is close to the experimentally determined value of 0.85 (Fig. 5).

3. Squall-line simulations

Here we reconsider the degree to which the above-described concept of cold-pool–shear interaction is applicable to understanding numerical simulations of squall lines. We first consider the basic influence of shear on the overall structure of the squall lines, in terms of cellular characteristics and line-averaged system evolution. We then offer several possible measures of overall squall-line strength to establish the degree to which

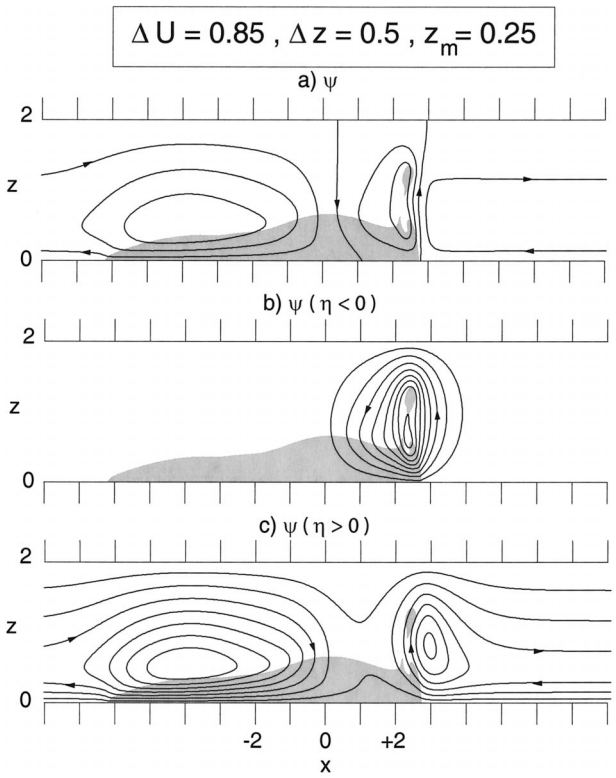

FIG. 10. Decomposition of the (a) flow field [ψ, contour interval (c.i.) = 0.1] into that induced by the vorticity associated with the (b) downshear cold pool [$\psi(\eta < 0)$, c.i. = 0.05] and that induced by the vorticity of the shear layer and the (c) upshear cold pool [$\psi(\eta > 0)$, c.i. = 0.05].

given environments could be considered more or less favorable. In view of the discussion given in the introduction, we consider the effects of shear depth and magnitude, as well as the solution sensitivity to the location of the shear layer relative to the surface.

a. Experimental design

Squall lines are simulated herein using the Klemp–Wilhelmson (1978) cloud model within a domain 600 km in the east–west (cross line) and 160 km in the north–south (along line) direction, with periodic conditions specified at the northern and southern boundaries. Grid spacing is 1 km in the horizontal direction and 500 m in the vertical direction. The top of the domain is set at 17.5 km AGL, where a gravity wave radiation condition is applied. Such resolutions are considered sufficient for simulating convective system structure and evolution (e.g., Weisman et al. 1997; Adlerman and Droegemeier 2002), and are consistent with the many recent squall-line simulation studies in the literature that are compared to the present results (e.g., Fovell and Ogura 1989; Fovell and Tan 2000; Lafore and Moncrieff 1989; Trier et al. 1997; Grabowski et al. 1998; Coniglio and Stensrud 2001). Only warm rain microphysics are employed, and the Coriolis force is set to zero. The exclusion of ice processes limits the interpretation of certain quantitative aspects of the present simulations, such as the extent and quantity of stratiform precipitation, and, to some degree, resultant cold-pool strengths. However, past studies (e.g., Fovell and Ogura 1988; Skamarock et al. 1994) suggest that these effects do not significantly impact the fundamental processes and relationships discussed herein. A free-slip condition is applied at the surface, which could impact the interpretation of surface wind production in the simulations (e.g., Adlerman and Droegemeier 2002), but, again, there is no evidence that this simplification fundamentally alters the system-scale relationships being considered.

The present experimental design is similar to that used by WKR, with the exception of both finer resolution (previously 2-km horizontal and 750-m vertical grid spacing) and a much larger domain (600 km versus 160 km) in the cross-line direction. We have found that the use of such large cross-line dimensions is critical for accurately representing the mature structure of the simulated systems, as important circulation-forcing regions at the rear of the system, associated with the cold pool at the surface and warm pool aloft, can be lost through the boundaries using smaller domains. In particular, Fovell and Ogura (1989) have noted that the degree of decay evident in the weaker shear simulations of RKW and WKR may have resulted from the constrained domain sizes in those earlier simulations, rather than from an actual physical process. We have found that the use of 600-km cross-line domains is sufficient to avoid this numerical effect over the 6-h integration period.

The horizontally homogeneous initial state is characterized by a single profile of temperature and moisture (Fig. 11a), as previously used by WKR, which has a convective available potential energy (CAPE) of 2200 J kg^{-1}. This amount of CAPE is most applicable to studying severe, midlatitude squall lines (e.g., Bluestein and Jain 1985), but recent studies of tropical systems (e.g., Trier et al. 1997; Robe and Emanuel 2001) suggest that the present relationships are applicable to tropical thermodynamic environments as well. Eight basic unidirectional wind shear profiles are considered (Fig. 11b), the first four representing 2.5-, 5-, 7.5-, and 10-km-deep surface-based shear layers, and the next three representing the 2.5-, 5-, and 7.5-km-deep shear cases with the shear layers now begining at 2.5 km AGL. Finally, for a few selected cases, the shear layer begins at 5 km AGL, to accentuate the differences between the surface-based and elevated shear cases. The magnitude of the wind speed difference across the shear layers, U_s, is varied from 0 to 40 m s^{-1}, representing much of the range of environmental shear conditions associated with squall lines.

The squall lines are initiated using a north–south-oriented line thermal of 1.5-K maximum potential temperature excess, with small (0.1 K) random potential

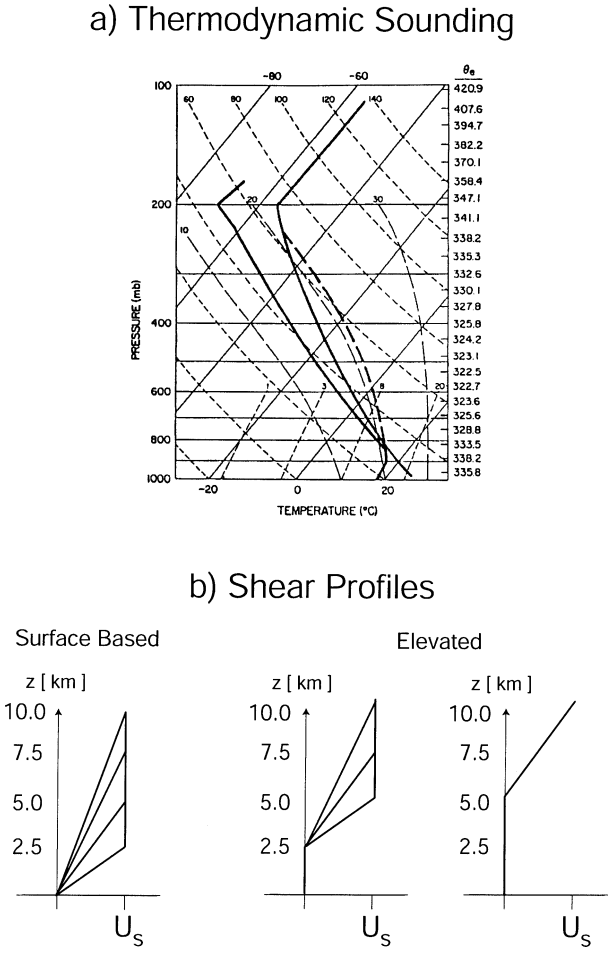

FIG. 11. (a) Thermodynamic sounding and (b) wind profiles used for simulations.

temperature perturbations added to the line thermal to allow for the development of three-dimensional features along the line. This potential temperature perturbation was the minimum necessary to trigger convection in a reasonable amount of time (1 h) for the vast majority of cases, and is small compared to the maximum potential temperature excess of 8 K for an undilute surface air parcel based on the environmental sounding (e.g., Fig. 11a). It was necessary to increase the initial thermal perturbation to 2.0 K for many of the $U_s = 30$ m s^{-1} cases, and 2.5 K for some of the $U_s = 40$ m s^{-1} cases, in order to allow the initial convection to develop in a similar amount of time compared to the weak- and moderate-shear simulations. However, this small difference in initiation procedure does not impact the basic conclusions drawn herein.

b. Squall-line structure–shear dependencies

The simulated squall lines all evolve through the phases of evolution shown schematically in Fig. 2, as the convectively generated cold pools strengthen over time. However, the time period over which this evolution takes place is inversely proportional to the overall magnitude of the ambient shear, with the weakest-shear simulations developing an overall upshear-tilted structure within the first couple of hours and the strongest-shear simulations maintaining a predominantly downshear-tilted structure throughout the 6-h integration period.

First, we investigate the role of surface-based environmental shear (e.g., Fig. 11b) on squall-line structure. The basic shear dependence is represented in Figs. 12 and 13, which depict along-line averaged vertical cross sections and horizontal cross sections at 3 km AGL of key storm properties at 4 h for the $U_s = 0$, 10, 20, and 30 m s^{-1}, 5-km-deep surface-based shear profiles, respectively. For the case with zero ambient shear (Figs. 12a, 13a), the system structure at 4 h is highly disorganized, with scattered, short-lived, convective cells far behind the leading edge of the spreading cold pool. With $U_s = 10$ m s^{-1} over 5 km AGL (Figs. 12b, 13b), the simulated squall line is more organized, with a larger number of weak convective cells scattered behind the leading edge of the surface cold pool, but it still exhibits a predominantly upshear-tilted configuration, with an ascending flow branch spreading predominantly rearward over a strong cold pool and divergent outflow at the surface. As the ambient shear increases to $U_s = 20$ m s^{-1} over 5 km (Figs. 12c, 13c), the system-scale updraft remains stronger and more upright, with the updrafts and rain cells forming a more continuous line along and just behind the leading edge of the surface cold pool. Additionally, a more symmetric anvil outflow is evident aloft. Finally, for $U_s = 30$ m s^{-1} over 5 km (Figs. 12d, 13d), the system-scale updraft remains upright-to-downshear tilted through most of the simulation, with strong, highly three-dimensional cells, some with supercellular characteristics, extending along the leading edge of the cold pool. A predominantly downshear-tilted anvil is now evident aloft.

Figure 14 presents close-up vertical cross sections of the cold pools for these cases at representative locations along the line at 4 h. Consistent with the results for the more simple streamfunction model presented in section 2 (e.g., Figs. 4, 6, 7), cold-pool depth (and strength) increases with increasing shear up to some optimal state (e.g., $U_s = 20$ m s^{-1} for these simulations), but decreases if the shear is increased even further. Of course, for these more complete simulations, cold-pool depth, strength, and shear magnitude are not independent parameters; for example, the subsequent strength of the convection, which depends on the shear, influences the subsequent strength/depth of the cold pool, etc. Still, we believe that the simple model offers important insights into the cold-pool behavior observed in the more complicated model.

The time series of maximum vertical velocity for these cases (Fig. 15a) shows that significant updrafts are being produced out to 6 h for all shears considered,

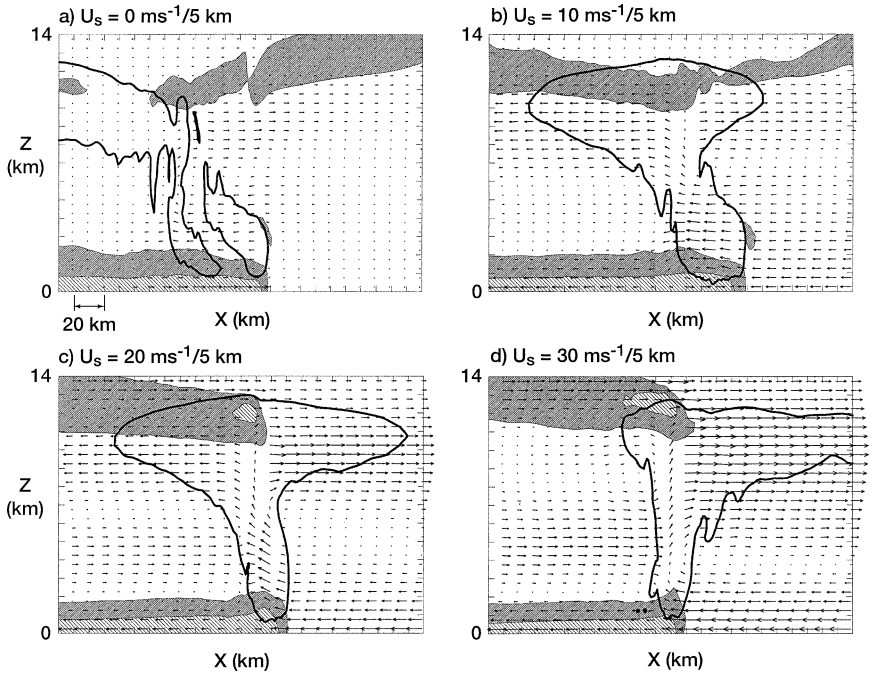

FIG. 12. Line-averaged vertical cross section of system-relative flow vectors, negative buoyancy field, and outline of the cloud field (thick line) for the (a) $U_s = 0$ m s^{-1} (b) $U_s = 10$ m s^{-1}, (c) $U_s = 20$ m s^{-1}, and (d) $U_s = 30$ m s^{-1} 5-km-deep surface-based shear simulations at 4 h. Magnitudes of the buoyancy field between -0.01 and -0.1 m s^{-2} are darkly stippled, with magnitudes less than -0.1 m s^{-2} lightly stippled. Vectors are included every 10 km in the horizontal, and 500 m in the vertical, with a horizontal vector length of 10 km equal to vector magnitude of 15 m s^{-1}. Tick marks are included every 10 km in the horizontal and 1 km in the vertical. Only a 240 km $\times$ 14 km portion of the full domain is shown.

but also shows that the average maximum strength of the updrafts clearly increases for increasing magnitudes of shear, as reported in previous studies (e.g., Thorpe et al. 1982; WKR). This positive role of shear is even more pronounced in the 20-min averaged rain rates (Fig. 16a), where the $U_s = 20$ and 30 m s^{-1} rain rates far exceed those for the weaker shears. The regeneration of significant updrafts through 6 h for the $U_s = 0$ and 10 m s^{-1} cases is a departure from the results of RKW and WKR, wherein the development of an upshear-tilted structure resulted in far more weakening of the subsequent convection. As noted above, we believe that this previous result was an artifact of the numerical design, as simulations were run too long on domains that were too small. However, consistent with RKW and WKR, the new results shown in Figs. 12 and 13 indicate that the convection for the weaker shear cases is still widely scattered behind the spreading cold pool, and is far less organized as compared to the behavior of the convective cells in the stronger-shear cases. Consequently, the rain rates (Fig. 16a) are also far less for these weaker shears.

The relative importance of the depth of the ambient shear layer is demonstrated in Fig. 17 for the $U_s = 20$ m s^{-1} surface-based shear cases. When the shear layer is confined to the lowest 2.5 km AGL, the system structure is similar to the 5-km-deep shear case. (cf. Fig. 12c with Fig. 17a). Additionally, very strong bow-shaped updraft segments at 3 km AGL are now evident along the line (Fig. 17b), with accompanying line-end vortices and locally intense rear-inflow jets, as previously described by Weisman (1993). It is interesting that the maximum vertical velocities for the 2.5-km shear case (Fig. 15b, thick line) are actually weaker than for the 5-km shear case (Fig. 15a, medium line), although the rain rates are quite comparable (e.g., Fig. 16). As also discussed by Weisman (1993), maximum vertical velocities are often weaker for such organized bow echoes, due to the interactions with the elevated rear-inflow jet, which forces the updraft current rearward above the jet level (usually 3–6 km AGL). However, updrafts are still very strong below this level, resulting in very large rain rates. When the shear layer is spread over the lowest 7.5 km AGL (Fig. 17c), the system now maintains a downshear spreading anvil aloft, but a more upshear-tilted structure at lower levels, with a shallower surface cold pool and a shallower front-to-rear ascending updraft current. Individual updrafts and rain cells at 3 km AGL are now scattered behind the leading edge of the surface cold pool (Fig. 17d), and are much weaker and disorganized than for the 2.5-km-depth shear case (Fig. 13c). The rain rates are also significantly reduced from the shallower-shear cases (e.g., Fig. 16), although, again

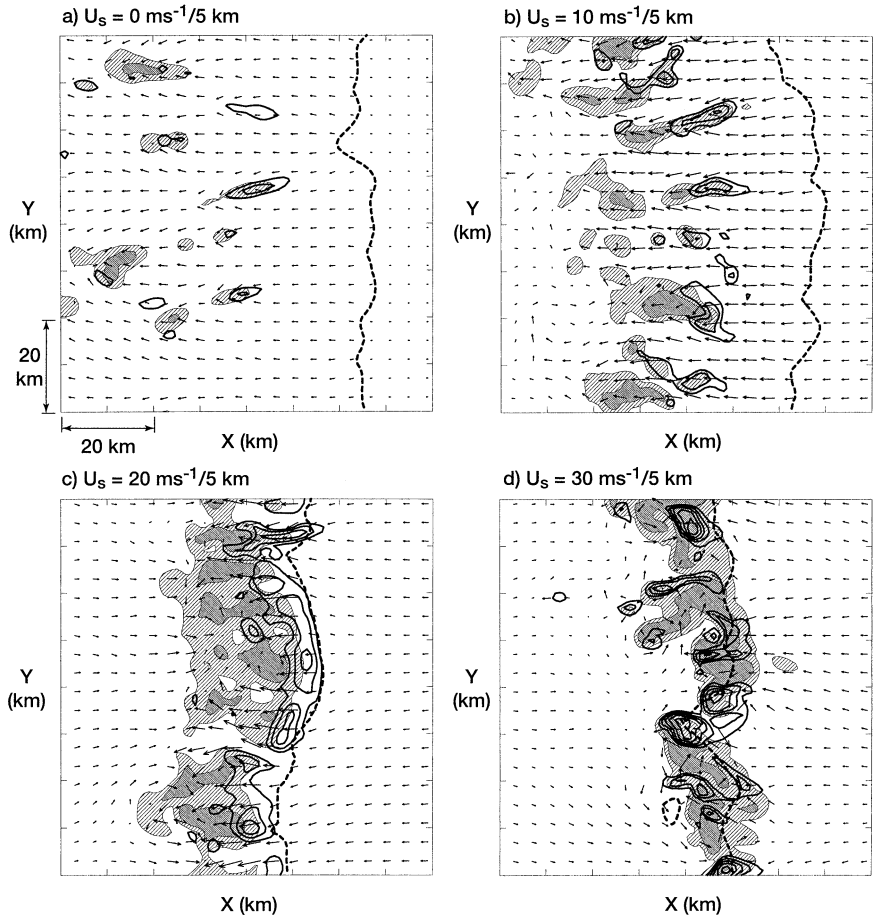

FIG. 13. Horizontal cross section at 3 km AGL of system-relative flow vectors, rainwater mixing ratio, and positive vertical velocity, for the (a) $U_s = 0$ m s^{-1}, (b) $U_s = 10$ m s^{-1}, (c) $U_s = 20$ m s^{-1}, and (d) $U_s = 30$ m s^{-1} 5-km-deep surface-based shear simulations at 4 h. Vertical velocity is contoured at a 3 m s^{-1} interval, with the rainwater lightly shaded for 0.001 to 0.004 g kg^{-1} and darkly shaded for greater than 0.004 g kg^{-1}. The surface cold-pool boundary, defined as the -1-K perturbation temperature contour, is depicted by the thick, dashed line. Vectors are included every 4 km in the horizontal, with a horizontal vector length of 4 km equal to a vector magnitude of 20 m s^{-1}. Tick marks are included every 10 km. Only an 80 km $\times$ 80 km portion of the full domain is shown.

maximum updrafts are comparable (e.g., Fig. 15). Thus, restricting a given net magnitude of shear (e.g., U_s) to shallow layers produces a stronger squall line than extending that shear over deeper layers.

A basic implication of the RKW theory is that ambient shear confined to the depth of the cold pool is most effective in countering the cold-pool circulation and thus promoting deeper cold-pool lifting. As shown in section 2 for a simple density current, if the shear layer is only above the top of the cold pool, the amount of lifting produced is significantly reduced (e.g., Fig. 5). Based on this, one would expect squall lines to be stronger and more long-lived if the shear layer were surface-based rather than elevated. Indeed, if the shear layer is located high enough, there would be virtually no interaction with the cold pool, and thus the overall system structure would revert more closely to the case with weak vertical wind shear. The effects of elevating the shear layer for the $U_s = 20$ m s^{-1} 5-km-deep shear case is presented in Fig. 18, where the shear layer is first located from 2.5 to 7.5 km, and then from 5.0 to 10.0 km AGL. As the shear layer is lifted, the system maintains more of a downshear-tilted anvil aloft, in response to the upper-level shear, but the low-level circulation becomes more upshear-tilted, with the convective cells becoming more scattered and located farther behind a shallower spreading surface cold pool. Rain rates are also far reduced from the comparable surface-based shear cases (e.g., Fig. 16). Thus, the overall system structure approximately reverts back to that associated with much weaker surface-based wind shears (cf. Figs. 18c,d with Figs. 12a, 13a).

As mentioned in the introduction, it has been proposed that the effect of shear (deep or shallow) is to

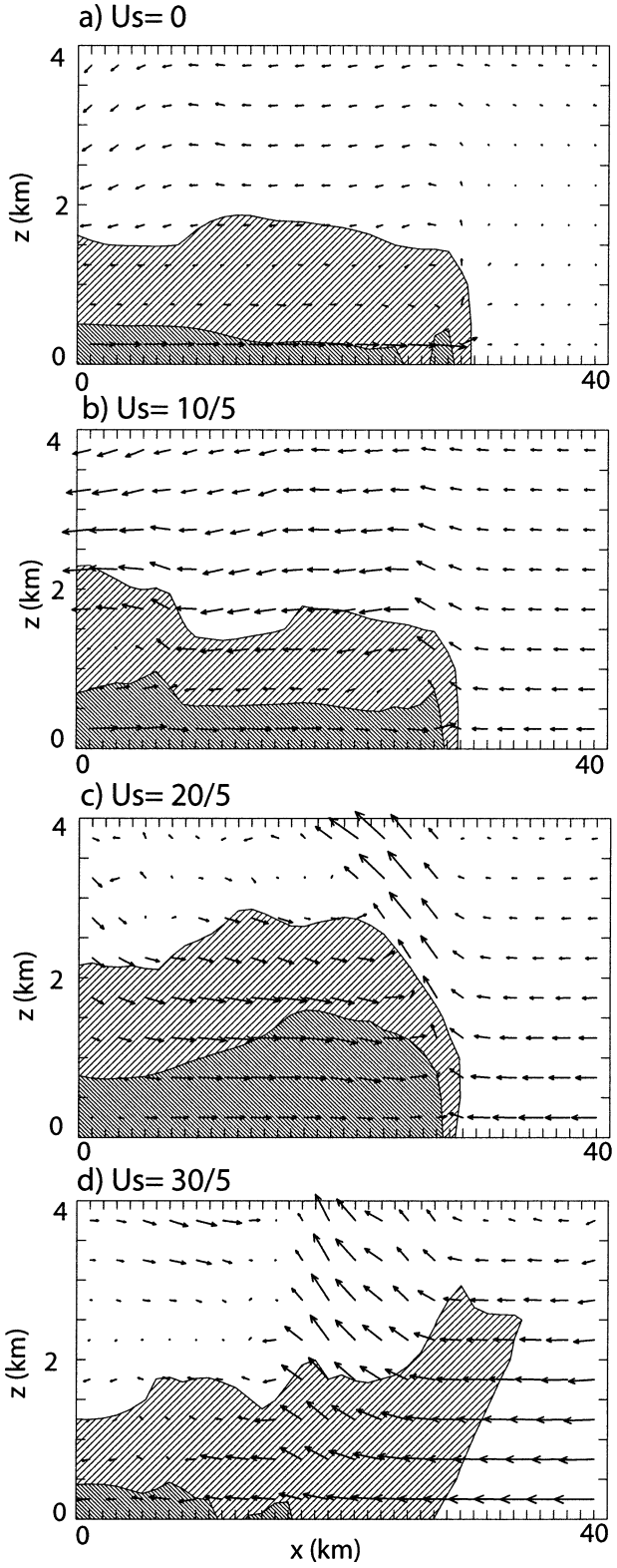

FIG. 14. Representative vertical cross section of system-relative flow vectors and negative buoyancy field through the cold pool for the (a) $U_s = 0$ m s^{-1}, (b) $U_s = 10$ m s^{-1}, (c) $U_s = 20$ m s^{-1}, and (d) $U_s = 30$ m s^{-1} 5-km-deep surface-based shear simulations at 4 h. Magnitudes of the buoyancy field between -0.015 and -0.15 m s^{-2} are lightly stippled, with magnitudes less than -0.15 m s^{-2} darkly stippled. Vectors are included every 2 km in the horizontal, and 500 m in the vertical, with a horizontal vector length of 2 km equal to vector magnitude of 15 m s^{-1}. Tick marks are included every 1 km in the horizontal and 500 m in the vertical. Only a 40 km $\times$ 4 km portion of the full domain is shown.

allow individual cells to move with the surface cold pool, thus enhancing cell strength and lifetime (e.g., Lafore and Moncrieff 1989; Thorpe et al. 1982; Moncrieff and Liu 1999). From this perspective, the low-level-shear–cold-pool interactions of RKW are not critical for system strength and longevity. Indeed, elevating the shear to 2.5 km AGL for the $U_s = 20$ m s^{-1} 5-km-deep shear simulation does produce an enhancement in system strength and organization compared to the zero shear simulation, although not to the extent observed when the shear is surface based. Some of this enhancement may be due to the influence that the circulation associated with the elevated shear may still be having on the circulation of the cold pool, as discussed in section 2a. Still, it is worth considering more carefully the role of the elevated-layer shear in maintaining or regenerating convective cells within such a system.

For the zero-shear case, new, weak cells are primarily initiated about 20 km behind the leading edge of the cold pool (e.g., Fig. 13a) by the collision of outflows from preexisting cells, which locally deepen the cold pool, thereby enhancing the lifting of the ambient air flowing rearward above the cold pool. The same process also contributes to cell regeneration somewhat for the $U_s = 20$ m s^{-1} elevated shear case. However, we find that lifting above the cold pool is additionally enhanced by the interactions of the elevated shear with the negative buoyancy regions of the preexisting raincells, as also described for low-level-shear–cold-pool interactions. This process is demonstrated in Fig. 19, which presents the early life cycle of a new convective element within the elevated shear-layer case shown in Figs. 18a,b. Initially, a preexisting raincell and associated downdraft are located about 20 km behind the cold pool (Fig. 19a). Air rises abruptly at the leading edge of the cold pool and then proceeds rearward for 10 to 20 km without any further significant ascent, consistent with the cold-pool circulation overwhelming the ambient low-level shear. Alternately, the lack of ascent at this stage can be attributed to downward-directed nonhydrostatic pressure gradient forcing associated with the cold-pool circulation, which counters the weak positive buoyancy forcing achieved through the lifting (e.g., Fovell and Tan 2000; Trier et al. 1997; Weisman et al. 1988). As the air parcels travel rearward, they encounter a negative buoyancy region that extends at least 3 km above the height of the cold pool, associated with the decaying raincell. Buoyancy in the cloud model is defined as

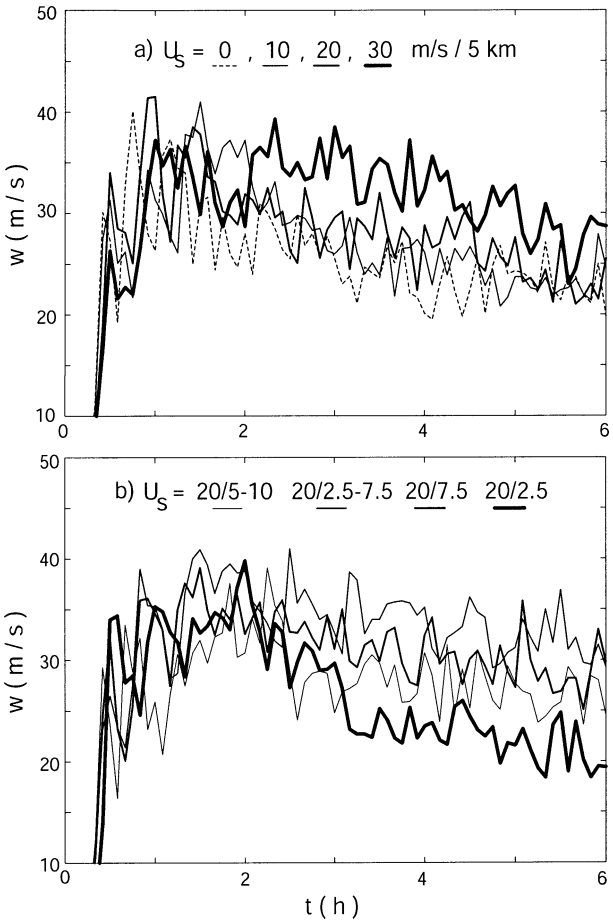

FIG. 15. Time series of maximum vertical velocity for the (a) U_s = 0, 10, 20, and 30 m s^{-1} over 5-km-deep surface-based shear simulations; and (b) U_s = 20 m s^{-1} over 2.5 km, U_s = 20 m s^{-1} over 7.5 km, U_s = 20 m s^{-1} over 2.5–7.5 km, and U_s = 20 m s^{-1} over 5.0–10.0-km-deep shear simulations.

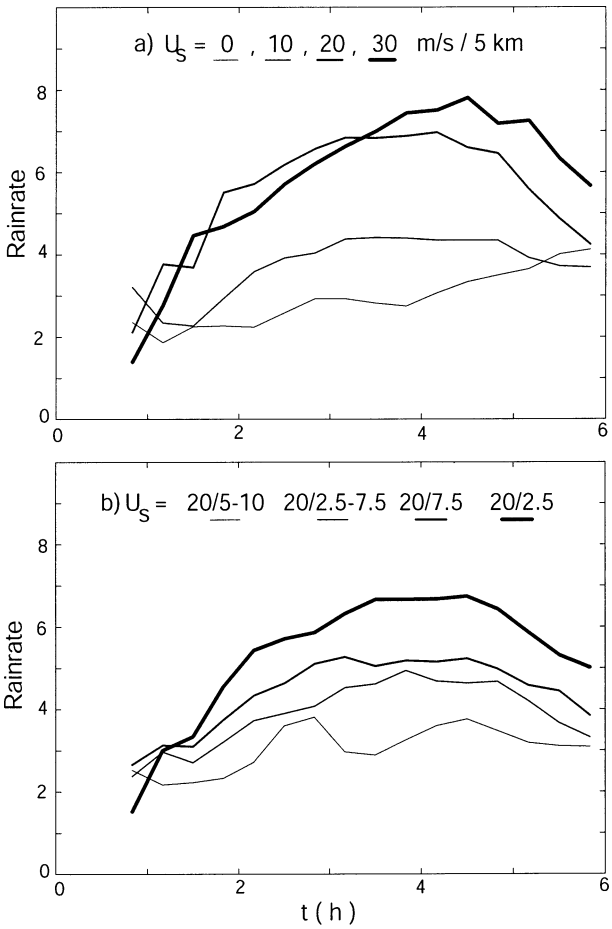

FIG. 16. Time series of rainfall rates [$\times 10^{10}$ kg (20 min)$^{-1}$] for the U_s = 0, 10, 20, and 30 m s^{-1} over 5-km-deep surface-based shear simulations; and (b) U_s = 20 m s^{-1} over 2.5 km, U_s = 20 m s^{-1} over 7.5 km, U_s = 20 m s^{-1} over 2.5–7.5 km, and U_s = 20 m s^{-1} over 5.0–10.0-km-deep shear simulations.

$$B \equiv g\left[\frac{\theta'}{\overline{\theta}} + 0.61(q_v - \overline{q}_v) - q_c - q_r\right], \qquad (9)$$

where $\overline{\theta}$ is the mean potential temperature; θ' is the perturbation potential temperature; and q_v, q_c, and q_r are the mixing ratios of water vapor, cloud water, and rainwater, respectively. This elevated negative buoyancy region is primarily associated with rain loading $-gq_r$, while at lower levels the negative buoyancy is primarily due to negative potential temperature perturbations resulting from evaporation. As the air parcels encounter this region, the interaction of the elevated shear with the positive horizontal buoyancy gradient enhances the lifting just ahead of the decaying raincell (Fig. 19b), leading to the subsequent development of a new convective cell (Fig. 19c).

This proposed process of enhanced cell regeneration for the elevated shear cases may not be the only process contributing in these cases, the details of which are beyond the scope of the present paper. In any event, our examination of new cell growth in all of these simulations shows no evidence that a preexisting convective updraft moving with the cold pool contributes to the cell regeneration process, as hypothesized in previous studies. In fact, the region of cell regeneration shown in Fig. 19 is characterized by downdraft prior to new cell growth (Fig. 19a). Further discussion of cell life cycles in simulated squall lines is presented in Fovell and Tan (2000).

The results for the full range of simulations are summarized in Table 1a, where the overall system-scale structure between 3 and 6 h is subjectively classified as either an upshear-tilted, multicellular system with cells scattered behind the leading edge of the cold pool (UP), a predominantly upright system with linear or bow-shaped segments of cells just behind the leading edge of the cold pool (B), or a system composed of more isolated, upright-to-downshear-tilted cells or embedded supercells right above the leading edge of the cold pool (D), as described in the earlier examples. It should be

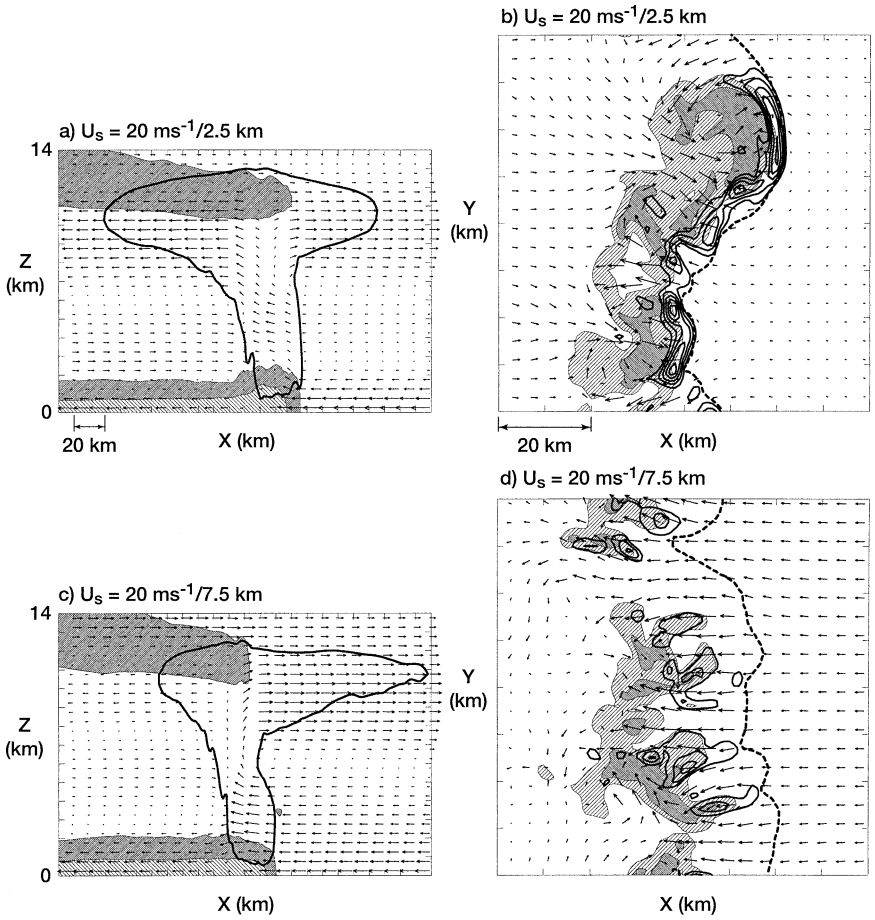

FIG. 17. Line-averaged vertical cross sections and horizontal cross sections at 3 km AGL at 4 h for the (a), (b) $U_s = 20$ m s^{-1} 2.5-km-deep and (c), (d) $U_s = 20$ m s^{-1} 7.5-km-deep surface-based shear simulations, as described for Figs. 12 and 13, respectively.

noted that the cases classified as either B or D include significant three-dimensional features embedded within the lines that could potentially limit the applicability of two-dimensional theories to interpreting overall system characteristics. This will also significantly impact comparisons with two-dimensional numerical models for this range of environments, as structures such as bow echoes and supercells cannot be reproduced in such models. Indeed, the inclusion of the third dimension releases the strong-shear constraint on squall-line strength noted in the two-dimensional studies of Hane (1973), Thorpe et al. (1982), and discussed by Lilly (1979, 1986), allowing for the development of long-lived convective structures that can gain energy from the shear. Despite such potential complications, a systematic change/increase in organization, from upshear to upright to downshear, for increasing magnitude of shear, is evident for all shear depth/location categories considered, consistent with the simple two-dimensional concepts suggested in Fig. 2. Additionally, more net shear (e.g., U_s) is needed to maintain an upright- or downshear-tilted system for the elevated versus surface-based shear cases, suggesting a reduced role of the elevated shear in contributing to system organization. Finally, well-organized bow echoes, as characterized in Fig. 17b, are most prevalent for the strong, shallow, surface-based shears, as found in Weisman (1993), although for slightly weaker shears than found in this previous study (e.g., bow echoes occur for $U_s = 15$ m s^{-1} over 2.5 km in the present study, while $U_s = 20$ m s^{-1} over 2.5 km was necessary in the previous study). These small differences are most likely related to both the finer resolutions and longer integration times used in the present study.

RKW and WKR classify overall squall-line strength and structure in terms of the parameter, $C/\Delta u$, where C represents the theoretical speed of propagation of a two-dimensional gravity current (e.g., cold pool; Benjamin 1968), given by

$$C^2 = 2\int_0^H (-B)\, dz, \tag{10}$$

where H represents the depth of the cold pool, B rep-

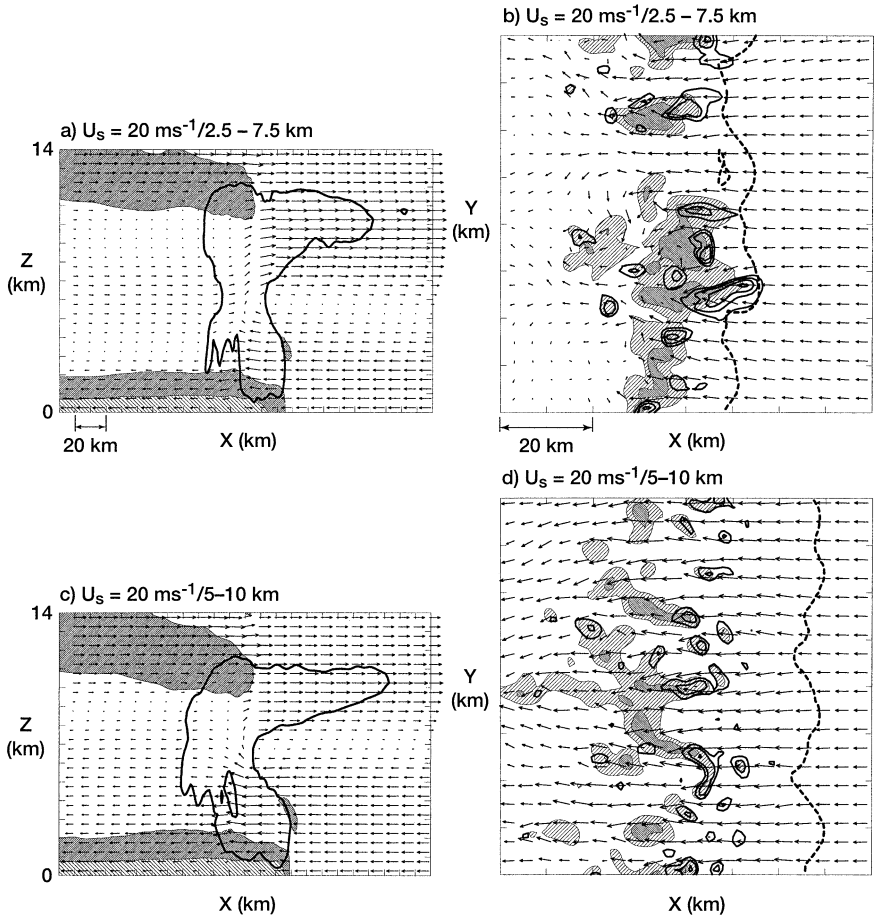

FIG. 18. Line-averaged vertical cross sections and horizontal cross sections at 3 km AGL at 4 h for the (a), (b) $U_s = 20$ m s^{-1} 2.5–7.5-km-deep and (c), (d) $U_s = 20$ m s^{-1} 5.0–10.0-km-deep elevated shear simulations, as described in Figs. 12 and 13, respectively.

resents the buoyancy defined in (9), and Δu is the ambient shear, given as the difference in line-perpendicular ambient wind between the surface and a level comparable to the depth of the cold pool. From the RKW perspective, a squall line takes on an overall upshear, upright, or downshear configuration for magnitudes of $C/\Delta u$ greater than, equal to, or less than 1, respectively, as depicted in Fig. 2.

Because of the critical importance of the cold pool in contributing to the structure and evolution of squall lines, we first present in Table 1b calculations of C representative of the mature phase of each of the simulations. For this purpose, the buoyancy field, B, is averaged along the line, and a representative cold-pool depth, H (defined as the level at which B vanishes), and minimum buoyancy, $B_{\min}$, is estimated for the 20-km region extending behind the leading edge of the cold pool. The buoyancy field is then assumed to decrease linearly to zero at height H, allowing for the following simplification of (10):

$$C^2 = -B_{\min} \times H. \qquad (11)$$

For the present purposes, C is calculated using (11) at 3, 4, and 5 h and then averaged over these three times to represent the average conditions observed during the mature phase of the present simulations; the standard deviation of C from the calculated average is small (1–2 m s^{-1}) over the time period included.

Table 1b reveals a maximum in resultant cold-pool strength for the $U_s = 15$–25 m s^{-1}, 2.5-km-deep surface-based shear cases. Here, C decreases for both weaker or stronger shears and also decreases for increasing shear depth. This enhancement in cold-pool strength for the shallowest shear examples is most directly related to an increase in cold-pool depth. A particularly interesting result is that C is significantly reduced for all of the elevated shear simulations. Analysis shows that the cold pools for the elevated shear cases are also characterized by higher values of θ_e, suggesting that the potentially coldest midlevel air is not reaching the surface as readily as for the surface-based shear simulations. Thus, the decrease in cold-pool strength for these elevated shear cases may be more related to the negative

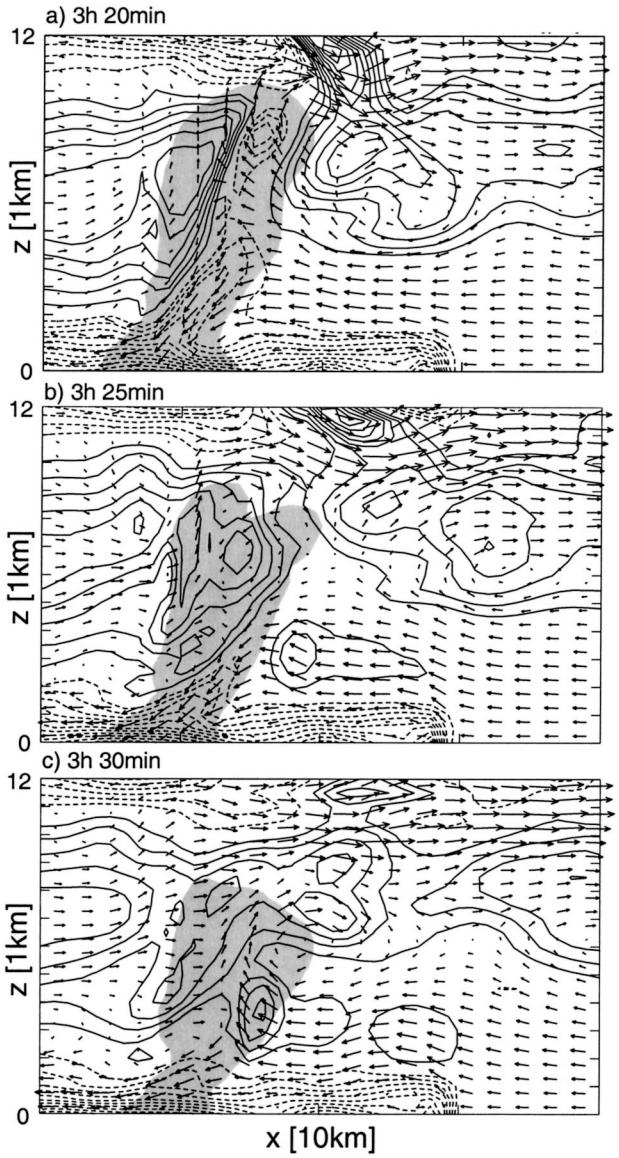

FIG. 19. Vertical cross sections of flow vectors, buoyancy, and rainwater at (a) 3 h, 20 min; (b) 3 h, 25 min; and (c) 3 h, 30 min through a developing convective cell for the $U_s = 20$ m s^{-1} 2.5–7.5-km-deep elevated shear simulation. Buoyancy is contoured at 0.02 m s^{-2} intervals, with rainwater mixing ratios greater than 0.001 g kg^{-1} shaded. Vectors are presented every other grid point in the horizontal direction, with a vector length of one grid point equivalent to a vector magnitude of 10 m s^{-1}.

influence of midlevel shear on the development of the system-scale downdrafts, rather than a direct consequence of cold-pool–shear interactions. The large variation in C among these simulations, all using the same thermodynamic sounding, underscores the complicated interdependence of this parameter with other aspects of system structure (e.g., RKW; Weisman 1992).

In Table 1c $C/\Delta u$ is presented for all of the simulations. In RKW and WKR, $C/\Delta u$ is calculated using a 2.5-km depth for the shear calculation. However, for the present simulations, a better correspondence with overall squall-line structure was obtained with Δu calculated over the lowest 5 km AGL, reflecting the ability of the shear in the 2.5–5-km layer to still contribute to cell regeneration somewhat, as shown in Fig. 19 ($C/\Delta u$ as calculated using a 2.5-km depth can be derived from Table 1c by multiplying the 5-, 7.5-, and 10-km-deep surface-based shear ratios by 2, etc.). Within this context, upshear-tilted systems generally occur for magnitudes of $C/\Delta u$ greater than 1.5 (averaged along the squall line between 3 and 5 h) with predominantly downshear-tilted systems occurring for $C/\Delta u$ less than 1. The most upright convective systems are found for $C/\Delta u$ between 1 and 1.5. As discussed by Lafore and Moncrieff (1989) and Weisman (1992), rear-inflow jets become a significant component of the system-scale circulation during the mature phase of many of these simulated squall lines, potentially complicating the simple $C/\Delta u$ relationships being espoused. In particular, Weisman (1992) showed that such rear-inflow jet could be incorporated into the present theory by including the vertical shear of the jet within the cold pool in the balance condition; for example, the appropriate ratio would now become $C/(\Delta u + \Delta u_j)$, where Δu_j represents the vertical shear within the cold pool. The simpler $C/\Delta u$ relationship, however, still provides a useful guide of overall system structure for a wide range of shear environments, emphasizing the general applicability of the original RKW concepts.

One of the concerns stated in Lafore and Moncrieff (1989) as to the application of $C/\Delta u$ concepts was that Δu may change significantly over time, as the convection begins to modify the ''environmental'' shear profile ahead of the system. Indeed, their Fig. 4a depicts significant modifications, especially above 6 km AGL, within such a two-dimensional squall-line simulation. This issue is highlighted further by Garner and Thorpe (1992), who, using a highly parameterized two-dimensional squall-line model, found even more substantial downstream modifications to the shear, extending to low levels as well. In order to address this concern for the present simulations, we computed vertical profiles of U averaged over an 80-km region ahead of the surface gust front, and also averaged along the line at 4 h (Fig. 20), for the $U_s = 0$, 10, 20, and 30 m s^{-1} over 5-km shear simulations discussed in Figs. 12, 13, and 14. As discussed by Lafore and Moncrieff (1989), the present results also show significant modifications of the shear profile above 6 km, primarily reflecting the upper-level downshear outflow circulation, which maximizes between 10 and 12 km AGL. However, the modifications to the shear are less than 1 m s^{-1} over the lowest 3.0 km AGL, with generally less than a 3 m s^{-1} modification between 3 and 6 km AGL for all the cases considered. Since the dependence of squall-line structure on shear is heavily weighted to the shear over the lowest 5 km AGL, and especially the lowest 2.5 km AGL, these environmental shear modifications will not significantly

TABLE 1a. System structure 3–6 h. UP: Upshear multicellular, B: Bow echo, and D: Downshear cells, supercells.

	Surface-based shear				Elevated shear (2.5 km)			(5 km)
U_s (m s^{-1})	2.5 km	5 km	7.5 km	10 km	2.5 km	5 km	7.5 km	5 km
0	UP							
10	UP	UP	UP	UP	UP	UP	UP	UP
15	B/UP	UP	UP	UP	UP	UP	UP	
20	B	UP/B	UP	UP	B/UP	UP	UP	UP
25	B	D/B	D	UP	D/B	D/UP	UP	
30	D/B	D/B	D	D/UP	D/B	D	D/UP	UP
40		D/B	D	D		D	D	

affect the $C/\Delta u$ relationships discussed above. These adjustments to the wind profile on the downshear side of the squall line are consistent with the theoretical arguments and numerical calculations of Fovell (2002), who also clarified that the more substantial modifications noted by Garner and Thorpe (1992) were an artifact of their simplified moisture parameterization scheme.

c. An ''optimal'' state

One of the primary goals of this paper is to revisit the concept of an optimal environment for squall-line strength and longevity. For the case of a cold pool spreading in a sheared flow, optimality is defined simply as the environment that produces the deepest, most upright lifting at the leading edge of the cold pool. From this perspective, an optimal state is envisioned when $C/\Delta u$, as presented in Table 1c, is close to 1. However, for full squall lines for which buoyancy is generated within the updrafts, and for which the resulting precipitating convective cells can have important feedbacks on the evolution of the cold pool, etc., the concept of optimality is not as clear-cut. What is optimal for the production of individually strong updrafts may not be the same as what is optimal for the production of strong downdrafts and surface winds, or surface precipitation. For example, a strongly sheared environment might be conducive to the development of a few strong, isolated supercells embedded within the line, but a more weakly sheared environment might be more conducive to the development of a more solid line of convective cells and overall heavier rainfall. It is the ability to produce a more solid line of convective cells rather than supercells that is specifically addressed by RKW. In order to address the variety of ways in which system optimality could be defined, Table 2 presents several commonly used parameters that measure various aspects of system strength.

Table 2a presents the total rainfall observed between 1 and 6 h for each simulation. The first hour is neglected here to avoid some of the differences due to the timing and strength of the initial sequence of cells among the various environments. Total rainfall increases significantly as the net shear (U_s) increases in magnitude for the 2.5- and 5-km surface-based shear simulations. However, total rainfall decreases significantly when the net surface-based shear (U_s) is spread over 7.5 or 10 km. Rainfall also decreases markedly for all of the elevated shear cases. All in all, the most optimal squall lines from this perspective are found for magnitudes of surface-based shear between $U_s = 20$ and 30 m s^{-1}, with the shear layer confined to the lowest 2.5 or 5 km AGL. Indeed, an ''optimization'' for the moderate surface-based shears would have even been more evident had we not increased the initial potential temperature perturbation to initiate convection for many of the $U_s = 30$ m s^{-1} or greater shear cases, better reflecting the ultimately negative influence of such strong shears on system development.

These results can also be interpreted to consider the effects of extending a layer of a given magnitude of shear over a deeper depth. For example, rainfall rates increase dramatically as a surface-based shear of $U_s = 10$ m s^{-1} over 2.5 km is deepened to $U_s = 20$ m s^{-1} over 5 km, but then decrease somewhat if the shear layer is deepened further to $U_s = 30$ m s^{-1} over 7.5 km or $U_s = 40$ m s^{-1} over 10 km. This result can also be

TABLE 1b. Average C (m s^{-1}) (3–5 h).

	Surface-based shear				Elevated shear (2.5 km)			(5 km)
U_s (m s^{-1})	2.5 km	5 km	7.5 km	10 km	2.5 km	5 km	7.5 km	5 km
0	19.0							
10	23.0	21.0	20.0	20.0	19.0	20.0	19.0	18.5
15	25.0	21.5	19.5	19.5	19.0	19.0	19.0	
20	26.0	25.0	20.0	20.0	18.0	18.5	19.0	18.0
25	25.0	23.0	19.0	19.0	19.5	18.0	19.0	
30	21.0	21.0	20.0	19.5	17.5	18.5	17.5	17.5
40		18.0	19.0	20.5		18.0	19.0	

TABLE 1c. Average $C/\Delta U_s$ (3–5 h).

	Surface-based shear				Elevated shear (2.5 km)			(5 km)
U_s (m s^{-1})	2.5 km	5 km	7.5 km	10 km	2.5 km	5 km	7.5 km	5 km
0	—							
10	2.3	2.1	3.0	4.0	1.9	4.0	5.8	—
15	1.7	1.4	2.0	2.6	1.3	2.5	3.8	
20	1.3	1.3	1.5	2.0	0.9	1.9	2.8	—
25	1.0	0.9	1.1	1.5	0.8	1.4	2.3	
30	0.7	0.7	1.0	1.3	0.6	1.2	1.8	—
40		0.5	0.7	1.0		0.9	1.5	

interpreted from the $C/\Delta u$ perspective presented in Table 1c. Starting with a suboptimal state ($C/\Delta u = 2.3$), deepening the shear layer produces a nearly optimal state ($C/\Delta u = 1.3$), but further deepening does not produce any additional benefit ($C/\Delta u = 1$). Similarly, if we extend the already nearly optimal $U_s = 20$ m s^{-1} over the 2.5-km shear case ($C/\Delta u = 1.3$) to a shear magnitude of $U_s = 40$ m s^{-1} over 5 km ($C/\Delta u = 0.5$), only slight enhancement in total rainfall is observed. From a two-dimensional perspective, one would expect this latter case with $C/\Delta u = 0.5$ to be weaker due to the exceptionally strong shear (indeed, the initial temperature perturbation had to be increased from 1.5 to 2 K to allow the convection for this case even to initiate). However, as previously discussed, the ability to develop more isolated, three-dimensional cells or supercells (given convective initiation) can mitigate the negative influence of the stronger shears.

As a similar integrated measure of system strength, Table 2b presents the total condensation observed from 1 through 6 h for each simulation, which was one of the primary measures applied in previous study of WKR. This parameter indicates a similar increase in overall system strength as the 2.5- or 5-km-deep surface-based shears increase from $U_s = 0$ to 20 m s^{-1}. As also shown for the total rainfall, total condensation decreases for either deeper or elevated shear layers, with virtually no enhancement beyond the zero-shear case evident if the shear layer is lifted to above 5 km AGL. These results differ somewhat from WKR, which showed a dramatic decrease in total condensation as the shear depth increased from 2.5 to 5 km AGL. However, as discussed above, these differences are directly attributable to the use of much smaller domains and coarser resolutions in WKR that restricted the ability to regenerate convective cells in the deeper shears and also to generate correctly system-scale features, such as rear-inflow jets.

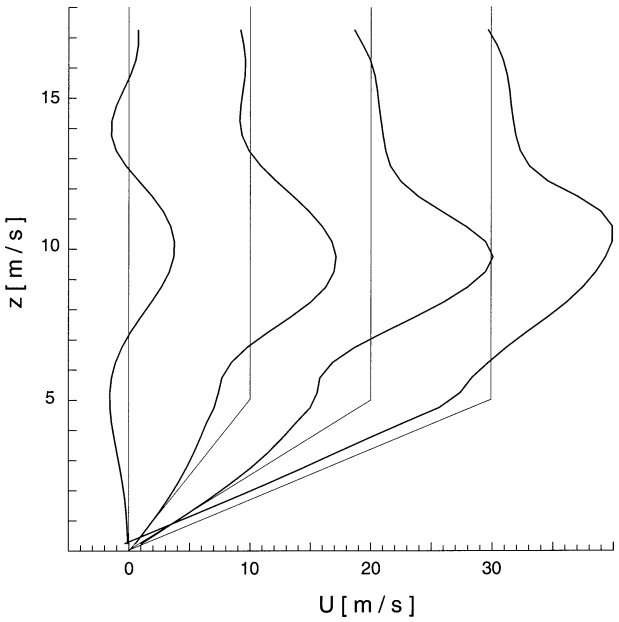

FIG. 20. Vertical profiles of the U component of the wind averaged along the line over an 80-km region ahead of the squall lines, for the (a)–(d) $U_s = 0$, 10, 20, and 30 m s^{-1} 5-km surface-based shear simulations, respectively.

As a measure of the ability of the given environment to produce strong, embedded convective cells over a long period of time, Table 2c presents the maximum vertical velocity observed between 3 and 6 h for each simulation. Like the previous parameters, maximum vertical velocity increases somewhat with increasing shear magnitude, but unlike the previous parameters, maximum vertical velocity also increases with shear depth and elevation. This result is most related to the tendency to produce more isolated convective cells for the deeper or elevated shear cases. Such isolated cells, which are more inherently three-dimensional, can be stronger than the more linelike updraft features evident for the shallower shears. Perhaps most surprisingly, the strongest individual cells occurred with the strong, elevated shear cases. These simulations were additionally characterized by weaker cold pools (e.g., Table 1b). Coniglio and Stensrud (2001) similarly found that the addition of upper-level shear could enhance longer-term updraft strength for idealized two-dimensional simulations. Hence, maximum updraft strength offers a significantly different perspective of optimality than the previously discussed parameters.

Finally, recent modeling and observational studies have also emphasized the potential for such convective systems to produce strong surface winds over long pe-

TABLE 2a. Total rainfall (1–6 h).

	Surface-based shear				Elevated shear (2.5 km)			(5 km)
U_s (m s^{-1})	2.5 km	5 km	7.5 km	10 km	2.5 km	5 km	7.5 km	5 km
0	0.44							
10	0.59	0.56	0.51	0.49	0.52	0.50	0.48	0.46
15	0.71	0.73	0.61	0.55	0.68	0.55	0.51	
20	0.83	0.86	0.68	0.61	0.60	0.60	0.56	0.46
25	0.86	0.89	0.73	0.66	0.77	0.64	0.59	
30	0.87	0.91	0.79	0.70	0.71	0.67	0.60	0.47
40		0.87	0.87	0.80		0.70	0.66	

riods of time (e.g., Weisman 1993; Coniglio and Stensrud 2001; Evans and Doswell 2001). Long-lived, severe wind-producing systems have often been associated with bow-echo-type structures embedded within larger convective systems. Table 2d presents both the average (averaged along the line and over time) and maximum U (east–west) component of the ground-relative wind at 250 m (the lowest grid level), based on the output at 3, 4, and 5 h, for each of the simulations. These results show that a broad range of shear conditions potentially support strong surface-wind production in these simulations, but the strongest average winds are generally produced for the 2.5–5-km surface-based shear cases, for shear magnitudes between $U_s = 10$ and 25 m s^{-1}. As shown in Table 1b these cases are also characterized by the strongest and deepest line-averaged cold pools, suggesting that the horizontal accelerations associated with the hydrostatic pressure excesses within the cold pools are significant contributors to strong surface-wind production in these simulations. This shear regime also includes as a subset the environments conducive to the development of well-organized bow echoes within the present simulations (e.g., Table 1a). However, potentially strong surface-wind-producing systems are not restricted to just such bow echo cases, but extend to more weakly and strongly sheared environments as well, as also noted in the previous simulations of Weisman (1993). It is also important to note that surface winds in both idealized simulations and observations increase in magnitude for increasing magnitudes of CAPE (e.g., Weisman 1993; Evans and Doswell 2001; Bluestein and Jain 1985; Bluestein et al. 1987), although this parameter is not varied in the present study.

Comparisons with more recent modeling and observational studies of severe wind-producing systems show much consistency with the present results. The Coniglio and Stensrud (2001) composite environment for a derecho event includes a magnitude of shear of 14–16 m s^{-1} over the lowest 5 km AGL, with much of this shear residing in the lowest 3 km, with an additional 15 m s^{-1} of shear between 5 and 10 km. Indeed, such an environment is well within the range of shears that produce long-lived swaths of potentially severe surface winds (defined here as maximum winds greater than 30 m s^{-1} at 250 m AGL) within the present simulations. Magnitudes of $C/\Delta u$ for their simulation (with Δu calculated over a 2.5-km depth) averaged about 2 during the mature phase of the system, and the overall system structure was composed of upshear-tilted updrafts with some embedded bow echoes. This is also reasonably consistent with the present simulations for which 15 m s^{-1} of shear over the lowest 2.5–5 km AGL represents a transitional regime between the more disorganized, upshear-tilted systems and more upright systems with embedded bow echoes. However, the present simulations also emphasize that stronger shears, especially when confined to low levels, produce even stronger, more coherent bow-echo-type structures and potentially even stronger maximum surface winds than the environment considered by Coniglio and Stensrud. Evans and Doswell (2001) found that 75% of the derecho events in their climatology had 0–6 km AGL shear magnitudes of greater than 11.6 m s^{-1}, with 25% of the cases having magnitudes greater than 20 m s^{-1}, also reasonably consistent with the present results. Their study, however, did not specifically address the association between shear and attendant convecctive organization.

TABLE 2b. Total condensation (1–6 h).

	Surface-based shear				Elevated shear (2.5 km)			(5 km)
U_s (m s^{-1})	2.5 km	5 km	7.5 km	10 km	2.5 km	5 km	7.5 km	5 km
0	1.16							
10	1.20	1.18	1.11	1.11	1.12	1.12	1.15	1.15
15	1.29	1.34	1.17	1.13	1.27	1.08	1.11	
20	1.37	1.45	1.20	1.17	1.20	1.12	1.12	1.12
25	1.40	1.46	1.18	1.16	1.26	1.09	1.11	
30	1.38	1.41	1.21	1.14	1.17	1.08	1.08	1.07
40		1.41	1.33	1.21		1.15	1.11	

TABLE 2c. W_{max} (m s^{-1}) (3–6 h).

	Surface-based shear				Elevated shear (2.5 km)			(5 km)
U_s (m s^{-1})	2.5 km	5 km	7.5 km	10 km	2.5 km	5 km	7.5 km	5 km
0	27							
10	30	30	29	29	31	33	31	32
15	29	35	34	33	36	37	34	
20	29	32	36	39	40	39	39	33
25	39	35	37	38	41	42	43	
30	39	38	38	38	40	40	42	42
40		38	35	38		38	41	

4. Summary and discussion

In the foregoing, we have addressed issues in the recent literature concerning the role of ambient vertical wind shear in controlling the structure, strength, and longevity of squall lines. A particular concern has been whether an appropriate balance between the cold-pool-generated circulation and the circulation associated with low-level ambient shear is a necessary requirement for sustaining most strong, long-lived squall lines, as suggested by RKW, WKR, and Rotunno et al. (1990), or whether other aspects of the shear profile, such as deeper or elevated shear layers could be as important in controlling system structure, strength, and longevity.

In order to address these concerns, we first revisited the basic premise of RKW theory, that the lifting produced at the leading edge of a spreading cold pool (density current) is ''optimized'' when the cold-pool circulation is countered by the opposite circulation associated with the ambient low-level vertical wind shear. A series of idealized density current simulations with a two-dimensional vorticity–streamfunction model were presented for a variety of shear magnitudes, depths, and elevations that reconfirm this basic idea, and add further support to the vorticity-balance interpretations originally presented by RKW.

In order to address the applicability of these concepts to interpreting full-physics cloud-model simulations of squall lines, we presented analyses from a large series of new idealized squall-line simulations with larger domains, higher resolution, and a wider range of environmental shear conditions than originally presented by RKW and WKR, including both deeper and elevated shear layers. As also discussed by Fovell and Ogura (1989), the use of large cross-line domains was found to be critical for accurately representing the mature system-scale structure. In particular, the abrupt demise of the weaker-shear, suboptimal squall lines in the more constrained-domain simulations of RKW and WKR thus appear to be more of a numerical artifact than a physical effect. This does not impact the overall influence of shear on system strength and structure as described in those previous papers. However, squall-line longevity, without reference to system strength and structure, is not found to be as sensitive to shear as in the past studies.

Using several different measures of system strength, the present results reconfirm that squall-line strength over a 6-h period is enhanced when moderate-to-strong shear is restricted to low levels, as found by Thorpe et al. (1982), RKW, and WKR, but now also extend the range of shear depths conducive to such enhancement from 2.5 to 5 km AGL. Increasing the surface-based shear depth to 7.5 or 10 km allowed for the development of strong, isolated convective cells along the line in the regime of moderate-to-strong shear, but such systems were weaker in terms of overall condensation and rainfall output. Locating the shear layer above 2.5 km AGL also allowed for significant, long-lived systems, although weaker and less organized than for the surface-based shears. Locating the shear layer above 5 km AGL, however, resulted in a much weaker and less-organized system, similar to the system obtained with no vertical wind shear.

It is also shown here that the ratio $C/\Delta u$ (with Δu calculated over the lowest 5 km AGL) offers a useful guide of overall squall-line structure for much of the range of shears considered, as previously presented by RKW and WKR, with predominantly upshear-tilted, up-

TABLE 2d. Avg/Max surface U (m s^{-1}) (3–5 h).

	Surface-based shear				Elevated shear (2.5 km)			(5 km)
U_s (m s^{-1})	2.5 km	5 km	7.5 km	10 km	2.5 km	5 km	7.5 km	5 km
0	14/23							
10	21/30	20/30	18/29	17/28	17/36	16/29	15/26	14/30
15	22/36	22/32	19/33	20/32	18/38	16/31	17/28	
20	22/37	22/35	20/37	20/34	16/40	16/35	16/33	16/28
25	21/40	19/42	18/33	20/35	13/37	13/31	17/31	
30	16/41	14/35	12/35	17/33	10/35	11/34	15/33	17/31
40		14/29	10/23	13/38		11/25	14/34	

right, or downshear-tilted structures occurring for magnitudes of $C/\Delta u$ greater than 1.5, 1–1.5, or less than 1, respectively. In terms of defining an optimal state for squall-line strength over the 6-h period based on a magnitude of $C/\Delta u$ approaching 1, it is clear that such a determination is open to reasonable differences of interpretation, depending largely on the parameters chosen as measures of such system strength. However, when considering the parameters that most nearly address the overall two-dimensional character of the convective systems (e.g., total rainfall, average surface wind, etc.), which is the true intention of the RKW approach, there is a strong degree of correspondence between the present cases that are more optimal from the $C/\Delta u$ perspective, and the tendency for the system to be composed of more erect, leading-line convection.

Some have interpreted the results of RKW and WKR as stating that a balance between the cold pool and ambient shear is ''necessary'' to support a strong, long-lived squall line. This seems inconsistent with the fact that significant, long-lived squall lines are frequently observed in weaker, suboptimal shear environments from the RKW perspective (e.g., $C/\Delta u$ greater than 1; Coniglio and Stensrud 2001; Evans and Doswell 2001). However, as stated in Rotunno et al. (1990), ''We recognize that systems that do not achieve an appropriate balance between the low-level shear and the cold pool strength may last a long time; however, we believe that in most instances, they will be weaker and shorter-lived than if the shear were in balance with the cold pool.'' We feel that the present expanded results add support to this conclusion. Significant, long-lived systems are produced over a wider range of environments than strictly ''optimal,'' but squall-line strength is clearly enhanced when moderate-to strong surface-based shear is confined to the lowest 2.5–5 km AGL. Perhaps the more important point, though, is that the relative strength of the cold pool and ambient shear has a profound effect on system organization over the entire range of environments considered, whether optimal or not, and, thus, represents a highly useful concept for describing overall system properties.

The present results were derived for an infinitely long squall line that was constrained to be perpendicular to the ambient shear in a thermodynamic environment most representative of severe, midlatitude squall lines. The same shear dependencies, however, can be derived by starting with isolated or short lines of convective cells, in both tropical and midlatitude environments alike. Starting in a horizontally homogeneous environment, such systems invariably reorient themselves to be perpendicular to the shear, through the continual regeneration of new cells along the cold pool, and, as with the present results, such regeneration is especially enhanced when the shear is confined to low levels (e.g., Weisman and Klemp 1986; Weisman 1993; Robe and Emanuel 2001). These results further confirm the generality of the RKW concepts in understanding the evolution of convective systems in a sheared environment.

An important step in judging the success of the present theory is whether it can be succesfully applied to describe real squall-line behavior. Within the realm of idealized simulations, environmental sensitivities can be systematically investigated, and an objective judgment can be rendered concerning the types of environments most conducive to system strength and longevity. Comparing such results to observations, however, can be particularly difficult, as observations are often quite sparse, and it is also difficult to differentiate the impact of external versus internal forcing mechanisms (e.g., given sufficient CAPE, a squall line can be long-lived by virtue of continual forcing from a synoptic-scale cold front, etc., independent of vertical wind shear conditions). Cold-pool characteristics are especially difficult to monitor over the lifetime of a system, and such input is critical for comparison with the above modeling results. One must also be careful to differentiate between the identification of environments that are in some way optimal for the maintenance of strong squall lines as compared to the identification of environments that are most often observed in association with the strongest, most long-lived systems. For instance, climatologically, environmental shear profiles are generally not restricted to low levels alone, so it is difficult to gauge the relative importance of low-level versus deeper-layer shear from observations. Studies such as Evans and Doswell (2001) have begun to address certain important aspects of squall-line climatology (e.g., the ability of such systems to produce strong surface winds) in a systematic manner, but far more work is needed, addressing the other aspects of squall-line structure discussed above. Direct comparisons between numerical simulations and observations are also made more difficult by ongoing uncertainties in the representation of many aspects of model physics, such as boundary layer processes, microphysics, etc. However, in cases when sufficient observations of system structure, cold-pool strength, vertical wind shear, etc., have been available, we believe that they have consistently confirmed the basic shear relationships discussed herein (e.g., see discussions in RKW, section 5, and WKR, section 8).

The fundamental issue addressed by RKW, WKR, and the present study is why environmental vertical wind shear promotes stronger, more long-lived squall lines. The fact that a certain amount of shear is beneficial to squall lines is not a point of controversy. The fact that low-level shear is especially beneficial to squall lines dates back to the earliest squall-line simulations studies of Thorpe et al. (1982), and has been consistently reproduced in all explicit squall-line simulation studies since. RKW specifically addresses and explains why such low-level shear is especially beneficial, but does not purport to explain every aspect of squall-line behavior. System-generated features, such as rear-inflow jets (e.g., Lafore and Moncrieff 1989; Weisman 1992)

or line-end vortices (e.g., Weisman and Davis 1998) are certainly important components of squall-line structure, but we find that even these features develop as a consequence of the simple cold-pool–shear relationships espoused herein, which we find represent the most fundamental internal control on squall-line structure and evolution.

Acknowledgments. We have benefited greatly from discussions and reviews of this manuscript by Drs. Stanley B. Trier, David C. Dowell, and Robert J. Trapp and three anonymous reviewers.

REFERENCES

Adlerman, E. J., and K. K. Droegemeier, 2002: Sensitivity of numerically simulated cyclic mesocyclogenesis to variations in model physical and computational parameters. *Mon. Wea. Rev.*, **130,** 2671–2691.

Benjamin, T. B., 1968: Gravity currents and related phenomena. *J. Fluid Mech.,* **31,** 209–248.

Bluestein, H. B., and M. H. Jain, 1985: Formation of mesoscale lines of precipitation: Severe squall lines in Oklahoma during the spring. *J. Atmos. Sci.,* **42,** 1711–1732.

——, G. T. Marx, and M. H. Jain, 1987: Formation of mesoscale lines of precipitation: Nonsevere squall lines in Oklahoma during the spring. *Mon. Wea. Rev.,* **115,** 2719–2727.

Byers, H. R., and R. R. Braham, 1949: *The Thunderstorm.* U.S. Government Printing Office, 287 pp. [NTIS PB-234-515.]

Coniglio, M. C., and D. J. Stensrud, 2001: Simulation of a progressive derecho using composite initial conditions. *Mon. Wea. Rev.,* **129,** 1593–1616.

Evans, J. S., and C. A. Doswell III, 2001: Examination of derecho environments using proximity soundings. *Wea. Forecasting,* **16,** 329–342.

Fovell, R. G., 2002: Upstream influence of numerically simulated squall-line storms. *Quart. J. Roy. Meteor. Soc.,* **128,** 893–912.

——, and Y. Ogura, 1988: Numerical simulation of a midlatitude squall line in two dimensions. *J. Atmos. Sci.,* **45,** 3846–3879.

——, and ——, 1989: Effect of vertical wind shear on numerically simulated multicell storm structure. *J. Atmos. Sci.,* **46,** 3144–3176.

——, and P.-H. Tan, 2000: A simplified squall-line model revisited. *Quart. J. Roy. Meteor. Soc.,* **126,** 173–188.

Garner, S. T., and A. J. Thorpe, 1992: The development of organized convection in a simplified squall-line model. *Quart. J. Roy. Meteor. Soc.,* **118,** 101–124.

Grabowski, W. W., X. Wu, M. W. Moncrieff, and W. D. Hall, 1998: Cloud-resolving modeling of cloud systems during Phase III of GATE. Part II: Effects of resolution and the third spatial dimension. *J. Atmos. Sci.,* **55,** 3264–3282.

Hane, C. E., 1973: The squall line thunderstorm: Numerical experimentation. *J. Atmos. Sci.,* **30,** 1672–1690.

Jirka, G. H., and M. Arita, 1987: Density currents or density wedges: Boundary-layer influence and control methods. *J. Fluid Mech.,* **177,** 187–206.

Klemp, J. B., and R. B. Wilhelmson, 1978: The simulation of three-dimensional convective storm dynamics. *J. Atmos. Sci.,* **35,** 1070–1096.

Lafore, J.-P., and M. W. Moncrieff, 1989: A numerical investigation of the organization and interaction of the convective and stratiform regions of tropical squall lines. *J. Atmos. Sci.,* **46,** 521–544.

——, and ——, 1990: Reply. *J. Atmos. Sci.,* **47,** 1034–1035.

Lilly, D. K., 1979: The dynamical structure and evolution of thunderstorms and squall lines. *Annu. Rev. Earth Planet. Sci.,* **7,** 117–161.

——, 1986: The structure, energetics and propagation of rotating convective storms. Part 1: Energy exchange with the mean flow. *J. Atmos. Sci.,* **43,** 113–125.

Moncrieff, M. W., and C. Liu, 1999: Convective initiation by density currents: Role of convergence, shear, and dynamical organization. *Mon. Wea. Rev.,* **127,** 2455–2464.

Newton, C. W., 1950: Structure and mechanism of the prefrontal squall line. *J. Meteor.,* **7,** 210–222.

Robe, F. R., and K. A. Emanuel, 2001: The effect of vertical wind shear on radiative–convective equilibrium states. *J. Atmos. Sci.,* **58,** 1427–1445.

Rotunno, R., J. B. Klemp, and M. L. Weisman, 1988: A theory for strong, long-lived squall lines. *J. Atmos. Sci.,* **45,** 463–485.

——, ——, and ——, 1990: Comments on ''A numerical investigation of the organization and interaction of the convective and stratiform regions of tropical squall lines.'' *J. Atmos. Sci.,* **47,** 1031–1033.

Simpson, J. E., 1997: *Gravity Currents in the Environment and the Laboratory.* Cambridge University Press, 244 pp.

Skamarock, W. C., M. L. Weisman, C. A. Davis, and J. B. Klemp, 1994: The evolution of simulated mesoscale convective systems in idealized environments. Preprints, *Sixth Conf. on Mesoscale Processes,* Portland, OR, Amer. Meteor. Soc., 407–410.

Smull, B. F., and R. A. Houze Jr., 1987: Rear inflow in squall lines with trailing stratiform precipitation. *Mon. Wea. Rev.,* **115,** 2869–2889.

Stoker, J. J., 1957: *Water Waves.* Interscience, 567 pp.

Thorpe, A. J., M. J. Miller, and M. W. Moncrieff, 1982: Two-dimensional convection in non-constant shear: A model of midlatitude squall lines. *Quart. J. Roy. Meteor. Soc.,* **108,** 739–762.

Trier, S. B., W. C. Skamarock, and M. A. Lemone, 1997: Structure and evolution of the 22 February 1993 TOGA COARE squall line: Organization mechanisms inferred from numerical simulation. *J. Atmos. Sci.,* **54,** 386–407.

Weisman, M. L., 1992: The role of convectively generated rear-inflow jets in the evolution of long-lived mesoconvective systems. *J. Atmos. Sci.,* **49,** 1826–1847.

——, 1993: The genesis of severe, long-lived bow echoes. *J. Atmos. Sci.,* **50,** 645–670.

——, and J. B. Klemp, 1986: Characteristics of isolated convective storms. *Mesoscale Meteorology and Forecasting,* P. S. Ray, Ed., Amer. Meteor. Soc., 331–358.

——, and C. A. Davis, 1998: Mechanisms for the generation of mesoscale vortices within quasi-linear convective systems. *J. Atmos. Sci.,* **55,** 2603–2622.

——, J. B. Klemp, and R. Rotunno, 1988: Structure and evolution of numerically simulated squall lines. *J. Atmos. Sci.,* **45,** 1990–2013.

——, ——, and W. C. Skamarock, 1997: The resolution dependence of explicitly modeled convective systems. *Mon. Wea. Rev.,* **125,** 527–548.

Xu, Q., 1992: Density currents in shear flows—A two-fluid model. *J. Atmos. Sci.,* **49,** 511–524.

——, and M. W. Moncrieff, 1994: Density current circulations in shear flows. *J. Atmos. Sci.,* **51,** 434–446.

——, M. Xue, and K. K. Droegemeier, 1996: Numerical simulation of density currents in sheared environments within a vertically confined channel. *J. Atmos. Sci.,* **53,** 770–786.

Xue, M., 2000: Density currents in two-layer shear flows. *Quart. J. Roy. Meteor. Soc.,* **126,** 1301–1320.

——, Q. Xu, and K. K. Droegemeier, 1997: A theoretical and numerical study of density currents in nonconstant shear flows. *J. Atmos. Sci.,* **54,** 1998–2019.